



Research article

Evaluation of bioactivity and antibacterial properties of Ti6Al4V-based green biocomposite implant encompassing TiO₂ nanotube arrays and garlic extract

Sadegh Jafari Jebeli, Rouhollah Mehdinavaz Aghdam^{*}, Aryan Najjari, Reza Soltani*School of Metallurgy and Materials Engineering, College of Engineering, University of Tehran, P.O. Box: 11155-4563, Tehran, Iran*

ARTICLE INFO

Keywords:

Ti6Al4V
TiO₂
Nanotubes
Garlic extract
Biocoating
Antibacterial

ABSTRACT

This study involved the incorporation of an antibacterial garlic extract into titanium oxide nanotubes (TNTs) formed via the anodization of Ti6Al4V implants. The garlic extract, obtained through low-temperature extraction aided by ultrasound waves, was loaded into the nanotubes. The presence of the nanotubes was confirmed through X-ray diffraction (XRD), energy-dispersive X-ray spectroscopy (EDS), and scanning electron microscopy (SEM). Fourier-transform infrared spectroscopy (FT-IR) and gas chromatography-mass spectrometry (GC-MS) were used to investigate the presence of bioactive compounds, particularly sulfur compounds responsible for garlic's antibacterial effects. The impact of loading two concentrations (0.1 and 0.2 g per milliliter) of garlic extract on *Escherichia coli* (*E. coli*) and *Staphylococcus aureus* (*S. aureus*) bacteria was examined. Results indicated a decrease in the growth range of *S. aureus* from 10⁹ to 10⁶ (CFU/ml) and *E. coli* from 10¹¹ to 10⁹ (CFU/ml) upon treatment. Additionally, cell adhesion and viability tests conducted on MG63 cells revealed an 8% increase in cell viability with the 0.1 g per milliliter concentration and a 35% decrease with the 0.2 g per milliliter concentration of garlic extract after 72 h of incubation (They have been evaluated by Microculture tetrazolium (MTT) assay). GC-MS analysis identified the presence of diethyl phthalate compounds in the garlic extract, suggesting a potential correlation with cellular toxicity observed in the sample with the higher concentration (0.2 g per milliliter) of garlic extract. Overall, the TNTs loaded with 0.1 g per milliliter of garlic extract simultaneously demonstrated antibacterial activity, cell viability, adhesion, and growth enhancement.

1. Introduction

The rapid advancement of modern technology and the global economy has led to significant improvements in the quality of life for the world's population over the past few decades. Nowadays, people enjoy much longer life expectancy, and it is expected that the population aged 65 and above will reach 21.1% of the global population by the end of the year 2050. Since elderly individuals are more susceptible to musculoskeletal disorders and dental problems, the aging population has resulted in an increased demand for hard tissue implants, including bone and dental implants [1–4]. On the other hand, everyday life injuries and car accidents often result in bone impairments such as fractures and fissures [5]. Additionally, specific bone disorders and surgical procedures can precipitate the

^{*} Corresponding author.

E-mail address: mehdinavaz@ut.ac.ir (R.M. Aghdam).

occurrence of bone defects. Large bone defects do not naturally heal with tissue growth; therefore, orthopedic implants are necessary [6]. In 2018, the orthopedic implant market in the United States achieved a noteworthy milestone, reaching a value of \$46.5 billion. Projections indicate that by 2026, this market is anticipated to witness a substantial growth, with an estimated value of \$64.0 billion [7].

Various materials have been investigated for the treatment of hard tissue defects. Active biopolymers such as poly (L-lactic acid) (PLLA) [8], polyglycolic acid (PGA) [9], collagen [10–12], and ceramics (hydroxyapatite (HA) [13] as well as tricalcium phosphate [14,15] and bioglasses [16] have demonstrated favorable outcomes in terms of bone or tissue growth. However, these materials are deprived of suitable mechanical properties due to their brittleness and low fracture strength [17]. In this regard, metallic materials, biologically neutral in response with excellent mechanical performance, are considered the most suitable materials [18]. Implants based on metals such as stainless steel, titanium-based alloys, and cobalt-based alloys are the most common orthopedic implant materials due to their cost-effectiveness, excellent durability, and desirable mechanical properties [7].

Among these materials, titanium alloys, particularly Ti6Al4V alloy, are one of the most widely used alloys due to their corrosion resistance, lightweight nature, low density, and non-magnetic behavior [19]. Additionally, Ti6Al4V almost entirely substitutes bones, tissues, or hardened structures, simulating them at the implantation site. Therefore, it finds applications such as dental implants, pacemakers, and fracture fixators. However, the Ti6Al4V alloy exhibits certain drawbacks such as lack of antibacterial activity and hemocompatibility, indicating cellular toxicity that could lead to implant failure. In fact, cellular toxicity is related to the toxic aluminum and vanadium ions released in the human body, potentially causing cell death, interference with bone mineralization, allergic reactions, Alzheimer's disease, microcytic anemia, and neurotoxicity [18,20,21].

Advancements in materials science and manufacturing technologies have significantly improved the success rate of implantation to approximately 90%. Nevertheless, premature implant failures due to improper bone integration with the implant, the body's immune response to foreign intrusion, and bacterial infections still necessitate further interventions [17]. Clinical reports indicate a failure rate of over 10% in the clinical application of bone implants, with 18% attributed to implant loosening and 20% to bacterial infections. Insufficient osseointegration activities in implants lead to slow bone growth and weak bone integration in the initial stages of implantation, potentially causing loosening or even implant dislodgement. Although implantation procedures are typically performed in sterilized environments, implants are susceptible to contamination by opportunistic bacteria that may have entered through inappropriate procedures or originated within the body. Bacteria adhered to the implant surfaces can form a biofilm that is challenging to remove and exhibits high resistance against antibiotics. Consequently, implants with osteogenic and antibacterial activities have garnered significant attention in recent decades [6,22,23].

This phenomenon not only escalates healthcare expenses but also precipitates limitations in bodily mobility, protracted hospital stays, heightened incidence of subsequent surgical procedures, potential necessity for organ excision, and in extreme scenarios, mortality. Typically, implantation is accompanied by systematic administration of drugs such as bone stimulants, anti-inflammatory, pain-relief, and antimicrobial medications. Systemic drug delivery for implant rejection has significant limitations. Blood is responsible for carrying systemically administered drugs to the intended site. The supply of blood to bone tissue is limited, so only 1% of the systematically prescribed drug reaches the intended location. Availability of the drug at the intended site necessitates prescribing higher drug concentrations for extended periods to achieve the required dosage at the specific location, potentially causing various side effects and reaching other tissues adversely. Another method, Local Drug Delivery (LDD), has found widespread application in orthopedics and dentistry. LDD offers several advantages over systemic drug delivery in implant-based treatments: Versatility in Drug Delivery, Optimal Drug Concentration, Personalized Treatment and Effectiveness due to Proximity [17,24–28].

Electrochemical anodization, or anodizing, is an appealing strategy that creates regular nanotubes on the surface of titanium, leading to the formation of a nanostructured tissue. These nanostructures are recognized for enhancing osteogenesis and can serve as controlled drug delivery reservoirs [22,29]. Titanium dioxide nanotubes (TNTs) are self-organized nanostructures in the form of tubular layers. They have gained significant attention in implant manufacturing due to their mechanical stability, low preparation cost, and superior biocompatibility compared to TiO₂ films. TNTs can create excellent nanostructured platforms with desirable transport pathways, strong adhesion to substrates, and high surface area, meaning they possess a large number of atoms available for interaction with various biological molecules on their surface [30].

Loading antibiotics into TNTs is one of the methods employed to enhance the antibacterial activity of these coatings. For example, gentamicin has been encapsulated within nanotubes to mitigate bacterial adhesion onto their surfaces. Investigations have revealed that the incorporation of gentamicin into nanotubes effectively inhibits bacterial adherence to the substrate, thereby impeding biofilm formation [31,32]. The misuse of antibiotics has resulted in a rise in antibiotic-resistant bacteria, notably Methicillin-Resistant *Staphylococcus aureus* (MRSA). The utilization of gentamicin-loaded nanotubes is frequently irrational, contributing to the development of reduced sensitivity among MRSA strains to these antibiotics. This has consequently rendered the treatment of implant-related infections more challenging, given the emergence of resistant strains. Furthermore, the substantial concentration of gentamicin around bone tissue has been associated with decreased osteoblast productivity, as well as constrained proliferation and differentiation of human bone marrow mesenchymal stem cells, thereby impeding the body's recovery process. Thus, it is imperative to research the development of an antimicrobial agent that is effective, safe, and applicable for loading into nanotubes to combat antibiotic-resistant bacteria [33].

Various materials ranging from chemical antibiotics to synthesized metal complexes, metal ions, and natural drug compounds have been utilized for the production of antimicrobial agents [34–38]. The use of natural medicinal compounds constitutes a comprehensive approach aimed at operating within the realm of natural bone therapeutics. Understanding the origins of these natural drugs in conjunction with clinical interventions, risk management, and regulations can facilitate a profound comprehension of their impact on tissue engineering. Incorporating contemporary artificial bone connections with active natural medicinal compounds at optimal

concentrations offers a promising avenue for mitigating potential adverse effects and fostering improvements in overall well-being, vitality, and lifespan [39]. One pivotal factor driving the urgent need for alternative treatments in the realm of infectious diseases is the widespread emergence of multi-drug resistant (MDR) bacteria, colloquially referred to as 'superbugs', alongside the formation of bacterial biofilms. This phenomenon severely compromises the effectiveness of conventional antibiotics, if not rendering them entirely ineffectual. Hence, the imperative arises for the swift development of alternative therapeutic modalities, particularly tailored for infections associated with biofilm formation. In recent times, considerable attention has been directed towards naturally occurring substances due to their notable antimicrobial properties and their propensity to circumvent the development of drug resistance. Among these, garlic emerges as a prominent example. *Allium sativum*, commonly known as garlic and a member of the Liliaceae family, enjoys widespread culinary use globally, particularly prevalent in regions such as Italy and Southeast Asia. Furthermore, garlic holds a venerable status in traditional medicine dating back to ancient civilizations. Its constituent compounds demonstrate a diverse array of antibacterial activities, thereby harboring significant potential for conversion into efficacious antibacterial agents. Studies have indicated that garlic extract (GE) manifests numerous biological activities, encompassing antibacterial, antiviral, antifungal, and antiparasitic properties, with notable emphasis on its effectiveness against multi-drug resistant bacterial strains and biofilm formations [40–42].

The aim of the present study is to improve the antibacterial properties of surfaces, prevent biofilm formation, and address the issue of antibiotic-resistant bacteria by creating a green nanostructured composite coating using the advantages of titanium oxide nanotubes and natural garlic extract. Titanium oxide nanotubes formed on Ti6Al4V implants act as reinforcing phases in nanocomposite coatings, enhancing the mechanical properties of the coating and serving as ideal reservoirs for controlled drug loading and release over time. On the other hand, garlic extract loaded into nanotubes plays the role of antimicrobial agent and biofilm inhibitor. In this study, the antibacterial properties of nanotubes containing natural garlic extract, along with their effects on the viability, growth, and adhesion of osteoblastic bone cells, were investigated.

2. Materials and methods

2.1. Materials

Medical implants of Ti6Al4V with a thickness of 1 mm were obtained from Nazari Titanium Company (Iran). Chemical compounds, ethylene glycol, ammonium fluoride, acetone, and 2-propanol, obtained from Merck (Germany).

2.2. Synthesis of titanium dioxide nanotube arrays via anodic oxidation method

The Ti6Al4V alloy was cut into square samples with dimensions of 1*1 mm. The surfaces of the samples were polished using sandpaper ranging from 320 to 2000 grit to achieve a shiny surface. Subsequently, the samples were immersed in deionized water (DI) (Tooska Shimi, Iran), 2-propanol, and acetone successively for 20 min in an ultrasonic bath to remove contaminants and grease. A single-step anodization process was carried out in a cell containing an anode, cathode, and electrolyte. The electrolyte consisted of a mixture of organic compounds (ethylene glycol), 1% by weight of NH_4F , and 2% by volume of DI water. Accordingly, in this study, for the synthesis of titanium oxide nanotubes on the surface of the implant, an electrolyte comprising 30 mL of ethylene glycol along with 0.333 g of ammonium fluoride salt and 0.6 mL of DI water was utilized. The Ti6Al4V alloy was selected as the anode and cathode, spaced 1 cm apart from each other, with a surface ratio of 2:1. The anodization process was conducted for 120 min under a constant voltage of 60 V. Post-anodization, to clean the surface of the nanotubes, the sample was subjected to ultrasound for 1 min and then air-dried at room temperature for 1 week.

2.3. Heat treatment of the nanotubes

The obtained samples from the anodization stage were annealed at 500 °C with a heating rate of 5 °C per minute for 120 min (The samples took 100 min to reach 500 °C and were then held at that temperature for 120 min) to induce the transformation of the titanium dioxide structure from the amorphous state to the crystalline state. This annealing process was crucial for enhancing the durability and adhesion between the substrate and the surface coating.

2.4. Preparation of garlic plant extract containing bioactive compounds

Due to the temperature sensitivity of the bioactive compounds in garlic extract, a low-temperature extraction method was employed. Fresh garlic was obtained from Hamedan city. The garlic cloves were separated and initially washed with tap water, followed by distilled water, and then disinfected with ethanol. Distilled water (DI) was chosen as the extraction solvent. To compare and investigate the effect of different drug concentrations, two different extraction ratios were utilized. The first ratio was 1 g of garlic to 5 mL of DI water, equivalent to a concentration of 0.2 g per milliliter. The second ratio was 1 g of garlic to 10 mL of DI water, equivalent to a concentration of 0.1 g per milliliter. Subsequently, garlic, along with the selected solvent, was placed in an industrial mixer for 3 min to obtain a homogeneous mixture. The extract was then transferred into a glass container and stored in the refrigerator at 4 °C for 24 h. To ensure the extraction of the desired compounds, the extract underwent ultrasonic bath treatment at a frequency of 28 kHz and power of 50 W for 30 min. It was then stored in the refrigerator for another 24 h, with occasional stirring. In the final step, the extract was centrifuged at 6000 rpm for 10 min at a temperature of 4 °C. The liquid portion passed through a filter and was preserved as garlic

extract for future use, stored in the refrigerator at 4 °C. The procedure used to obtain the garlic extract was accomplished through the utilization of methodologies previously investigated in prior research endeavors [43–45].

2.5. Loading garlic extract into titanium dioxide nanotubes

For drug loading into the formed nanotubes, the most common method involves pipetting the drug onto the sample surface and then drying it in a desiccator, repeating the process several times. However, due to temperature sensitivity and to ensure the successful loading of the drug into the nanotubes, a desiccator was connected to a vacuum pump. The vacuum allowed the drug to enter the nanotubes and facilitated the evaporation of the base solvent. In summary, to load a consistent amount of drug, the samples were immersed in the drug solution for 1 day. Subsequently, they were immediately placed in the vacuum desiccator for 1 h at room temperature (20–25 °C). To repeat the process, the drug was pipetted onto the sample surface and placed in the vacuum desiccator. This procedure was repeated 5 times. After the process, the samples were stored at 4 °C until the necessary analyses were conducted [46–48].

2.6. Characterizations

2.6.1. Surface morphology analysis using field emission scanning electron microscopy

The FESEM (Field Emission Scanning Electron Microscope) device (MIRA3 model, manufactured by TESCAN) was employed for imaging the surfaces of samples after the anodization process and drug loading. Subsequently, the acquired images were analyzed using ImageJ software.

2.6.2. Surface chemical analysis using energy dispersive X-ray spectroscopy

The FESEM device (MIRA3 model, manufactured by TESCAN) was employed for the extraction of elemental mapping and chemical analysis of samples.

2.6.3. Crystal structure analysis

To determine the crystal structure and existing phases in the anodized samples, X-ray diffraction analysis (XRD) was conducted using a Philips X'Pert Pro X-ray diffractometer with Cu- α radiation (wavelength of 1.5410 Å) and a step size of 0.02° at 40 kV. The obtained results were analyzed using X'Pert HighScore Plus software.

2.6.4. Fourier transform infrared analysis

To identify the compounds and bonds present in the loaded garlic extract on the surface of nanotubes, Fourier transform infrared (FT-IR) analysis was performed using The PerkinElmer Spectrum Two with the UATR.

2.6.5. Gas chromatography-mass spectrometry analysis

Gas chromatography-mass spectrometry (GC-MS) analysis was carried out to determine the quantities of individual compounds present in the prepared natural garlic extract. This analysis was performed using a GC-MASS AGILENT 7890A instrument to investigate the specific effects of each compound.

2.7. Antibacterial properties evaluation

For evaluating the antibacterial properties of the samples, the colony-forming unit (CFU) counting method was employed. Initially, representative strains of Gram-negative bacteria, *E. coli* (ATCC 25922), and Gram-positive bacteria, *S. aureus* (ATCC 25923), were prepared at a concentration of 10^5 CFU/ml. Subsequently, the prepared samples were exposed to these bacterial strains for 24 h. After this period, serial dilutions ranging from 10^{-1} to 10^{-20} were prepared from the treated and control samples and transferred to Petri dishes containing nutrient agar (Merck, Germany). The plates were then incubated at 37 °C for 24 h, and the formed colonies were counted for analysis.

2.8. Cellular evaluation

2.8.1. Cell proliferation

In this study, human osteosarcoma cells (MG63, NCBI 555C) obtained from the Pasteur Institute of Iran cell bank were utilized. After thawing the cells, they were transferred to flasks containing DMEM culture medium (Gibco, USA) supplemented with 10% Fetal Bovine Serum (FBS) (Gibco, USA) and incubated in a humidified atmosphere at 37 °C with 5% CO₂. It is noteworthy that the culture medium was replaced every 3–4 days. To assess the toxicity of the samples and their impact on cell growth and proliferation, a direct contact method was employed. The samples were sterilized by exposure to UV radiation for 45 min.

2.8.2. Microculture tetrazolium (MTT) assay

In this study, to assess cellular proliferation, 10^4 cells in 60 μ L of culture medium were placed on each of the samples inside the wells of a 24-well cell culture plate (SPL, Korea). Subsequently, after 4 h of incubation at 37 °C, the cells adhered to the sample surface. After ensuring cell adhesion, 300 μ L of culture medium were added to each well. After 1 and 3 days, the medium was aspirated from the

cells as much as possible, and 300 μL of MTT solution at a concentration of 0.5 mg/ml were added to each well and incubated for 4 h. After 4 h, the solution was removed from the cells, and isopropanol (Sigma Aldrich, USA) was added to dissolve the purple formazan crystals. To better dissolve the MTT precipitate, the plate was shaken for 15 min on a shaker device. Then, 100 μL of the purple solution corresponding to each well were transferred to a 96-well plate (SPL, Korea). The concentration of the dissolved substance in isopropanol was calculated at a wavelength of 570 nm using an ELISA reader (BioTek ELx 808, USA). Wells with higher optical density indicate a higher cell density. Therefore, equation (1) [49] allows the determination of the wells with higher cell counts, and comparisons were made with the control sample. It is essential to note that each sample was tested in triplicate.

$$\text{Toxicity (\%)} = \left(1 - \frac{\text{mean OD of the sample}}{\text{mean OD of control}} \right) \times 100 \quad \text{Equation (1)}$$

$$\text{Viability (\%)} = 100 - \text{Toxicity (\%)}$$

2.8.3. Cell adhesion assessment

To investigate cell adhesion, sterilized samples were placed in each well of a sterile 24-well plate. Subsequently, 20,000 cells in a volume of 100 μL were seeded onto each sample. The samples were then incubated for 4–5 h. After cell adhesion, a specific amount of cell culture medium containing 10% FBS was added to each well. After 24 h, the culture medium was removed, and the samples were rinsed with Phosphate-Buffered Saline (PBS) (Merck, Germany) for 30 s. Following rinsing, a 3.5% glutaraldehyde solution (Sigma Aldrich, USA) was utilized for cell fixation. Specifically, after applying a predetermined volume of fixative onto each sample, they were refrigerated for 2 h. Subsequently, the fixative was removed, and the samples were washed with deionized water and alcohol solutions of varying concentrations (50%, 60%, 70%, 80%, and 96%). Cell adhesion to the samples was examined using FESEM (MIRA3 model, manufactured by TESCAN).

3. Results and discussions

3.1. Investigation of morphology and surface chemistry after anodic oxidation process

3.1.1. Existing elements on the surface of the sample

After performing the anodization process, the first step to investigate the formation or absence of TNTs involves determining the elements present on the surface. For this purpose, EDS analysis was employed. Comparing the elemental composition on the surface of the sample before and after the anodization process elucidates the presence of TNTs on the surface (Fig. 1).

As observed in Fig. 1-A, the presence of Ti, Al, and V elements on the implant surface before annealing is expected. However, after annealing and the formation of TiO_2 nanotubes on the surface, a reduction in the percentage of these mentioned elements is noticeable. Moreover, the presence of oxygen with an approximate weight percentage of 31% (Fig. 1-B) increases the likelihood of TNT formation on the surface.

3.1.2. Surface microstructure analysis

The most effective way to confirm the presence of TNTs on the surface is to observe the sample surface. For this purpose, FESEM was employed. As illustrated in Fig. 2 and compared with references [33,46] it can be observed that nanotubes have been successfully formed on the surface of the implant. Fig. 2 (A-D) shows various magnifications including 8000, 60000, 200000 and 600000 respectively.

As expected, due to the biphasic structure of the Ti6Al4V implant, the formation of nanotubes at two different levels within the α and β phases is clearly observed in Fig. 2 (A and B) [50,51]. In Fig. 2 (C and D), the diameter and wall thickness of the nanotubes are clearly depicted.

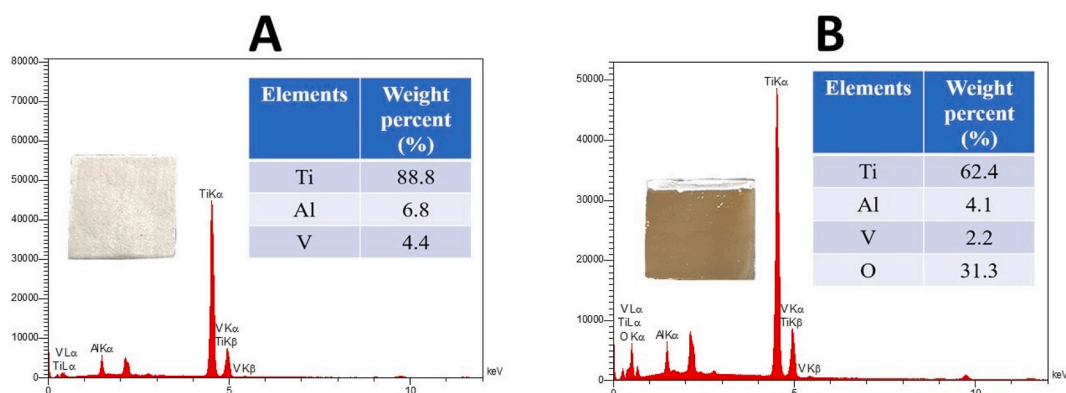


Fig. 1. EDS results from the surface of Ti6Al4V implant before (A) and after (B) anodizing.

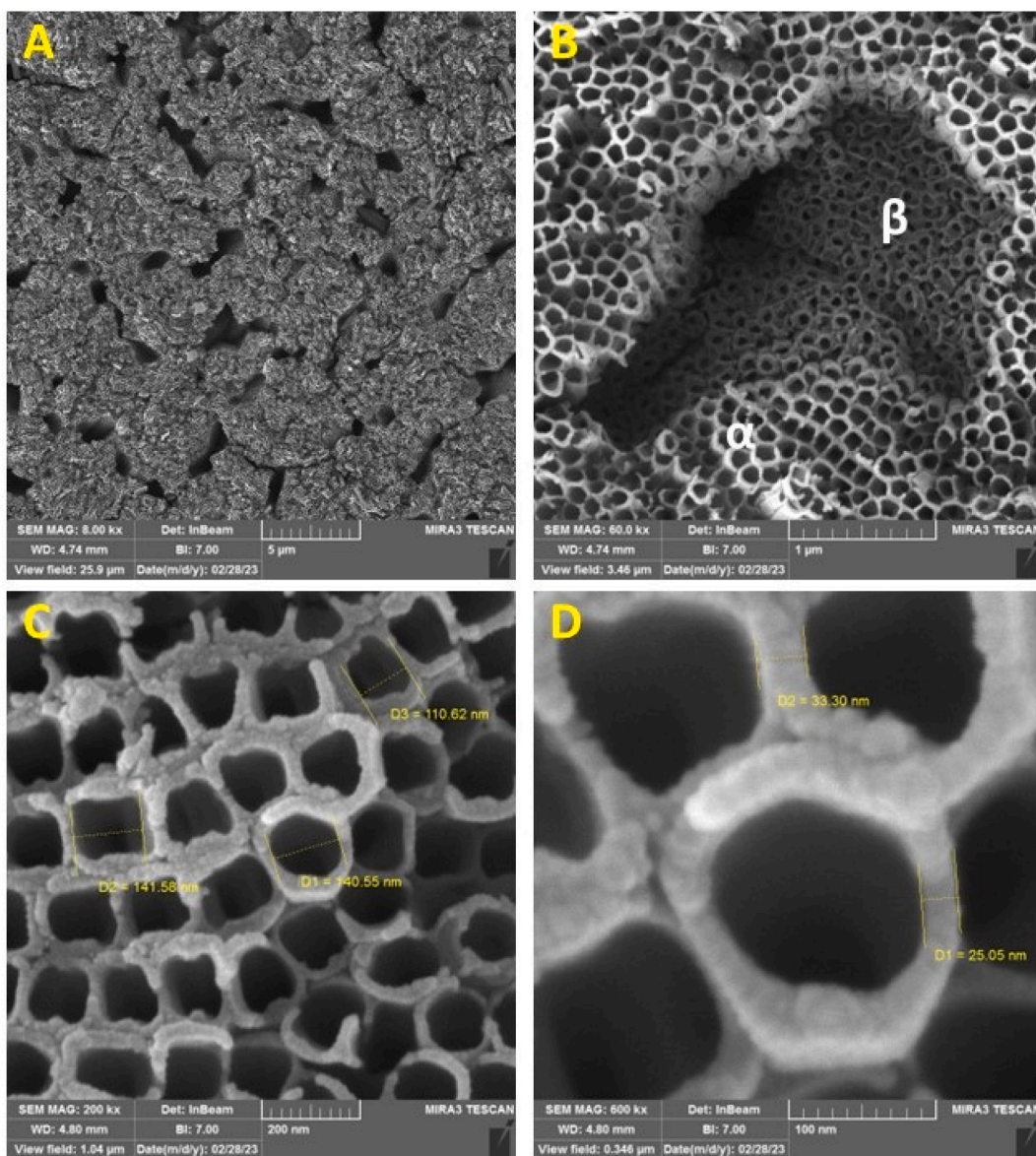


Fig. 2. FESEM images of anodized nanotubes on the surface of the Ti6Al4V implant at various magnifications including 8000, 60000, 200000 and 600000 (A-D respectively).

To view the nanotubes from different angles and determine the height of the formed nanotubes, which essentially indicates the thickness of the coating created on the surface, scratches were made on the surface of the implant. This was done to separate the nanotubes with their brittle oxide structure from the surface, enabling the observation of different orientations, as shown in Fig. 3.

As observed in Fig. 3-A, the nanotubes are separated from the surface and positioned around the scratch, delineated by green circles. Fig. 3-B provides a clear side view of the nanotubes, demonstrating their smooth and uniform walls. Under the conditions of 120 min of anodization and a voltage of 60 V, the nanotubes have a height of 7 μm . Fig. 3-C and 3-D indicate the bottom view of the nanotubes and the formed holes on the substrate as a result of separation of nanotubes respectively.

3.1.3. Heat treatment of the nanotubes

Nanotubes initially possess an amorphous structure. By subjecting the samples to heat treatments, it is possible to transform the amorphous structure into a crystalline anatase structure. The crystalline anatase structure enhances mechanical properties and adhesion [46]. It provides suitable photocatalytic properties, enabling easy sterilization of samples through ultraviolet radiation [52], and also exhibits excellent cellular activity [53]. XRD is employed to determine the formation of the anatase phase, the results of which are depicted in Fig. 4.

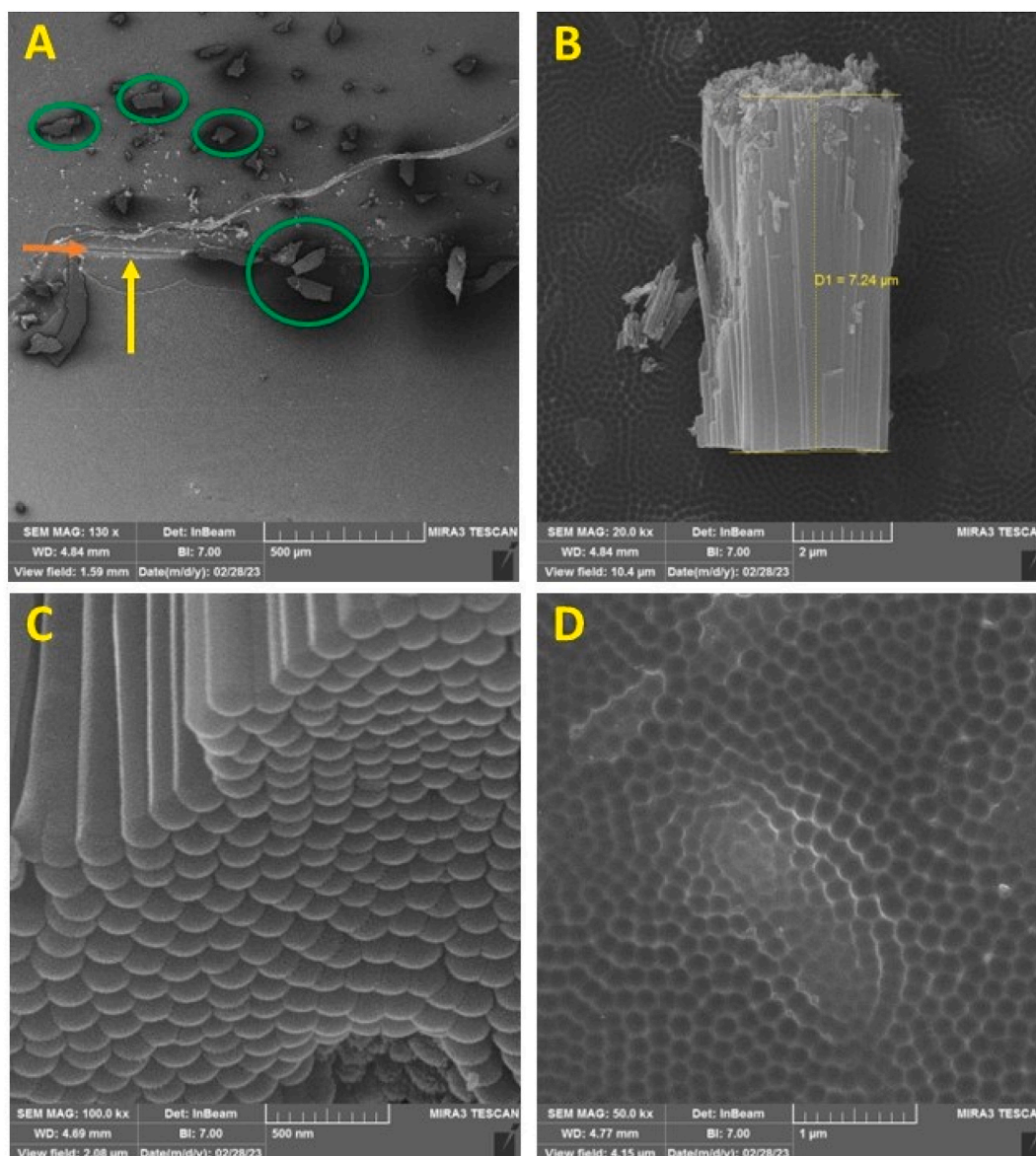


Fig. 3. FESEM micrographs of the anodized nanotubes on the surface of the Ti6Al4V implant are depicted in the images. (A) indicates the scratch created on the surface (orange arrow for the direction of the scratch and yellow arrow for the separated nanotube area), (B) shows a side view of the nanotubes, (C) displays the bottom view of the nanotubes, and (D) illustrates the holes formed on the substrate due to the separation of nanotubes. (For interpretation of the references to colour in this figure legend, the reader is referred to the Web version of this article.)

Graph B clearly illustrates the amorphous region originating from the primary structure of nanotubes at lower angles. As the X-ray diffraction angle increases, the depth of penetration also increases. Consequently, the peaks obtained from the crystalline planes of the substrate region, namely Ti6Al4V implants, are observed. Graph C shows the peaks resulting from the formation of anatase crystalline structure. The peaks occur at angles $2\theta = 25.28^\circ, 37.81^\circ, 47.99^\circ,$ and 53.95° corresponding to the planes (101), (004), (200), and (105) of the anatase crystalline structure [54,55]. Additionally, the planes of the α and β phases of the Ti6Al4V implants are also indicated in this graph [56].

3.2. Drug loading into the created nanotubes

After creating a nano-coating with a thickness of $7\ \mu\text{m}$ and successfully forming arrays of nanotubes on the surface, the next step involved loading natural drug compounds into the interior of these nanotubes. Garlic natural extract, prepared using a combination of available methods for drug loading into nanotubes (pipetting, immersion and using vacuum pump [46–48]), was transferred to the surface coating to create a green nanostructured bio-composite coating. To ensure the successful loading of the drug onto the sample

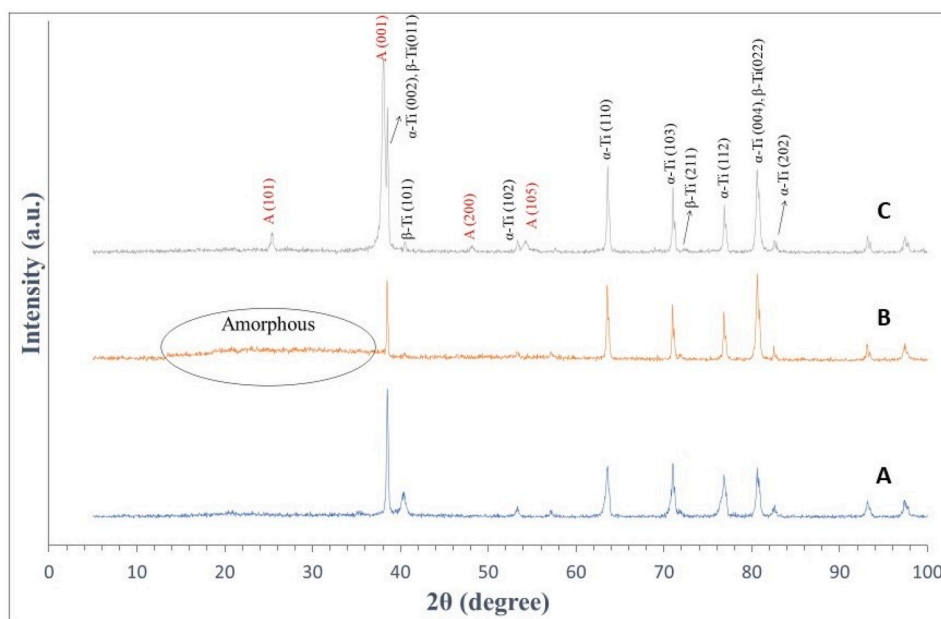


Fig. 4. XRD results of Ti6Al4V implant before anodizing (A), after anodizing (B) and after anodizing and heat treatment in 500 °C for 2 h (C).

surface, FESEM images and EDS analysis were conducted, as shown in Figs. 5–7.

Fig. 5 provides a view of the sample surface before (A) and after (B–D) drug loading. Fig. 5-B illustrates drug loading through immersion without applying vacuum; it is evident that drug compounds are heterogeneously deposited and accumulated on the surface, leading to non-uniform drug loading on many nanotubes. Additionally, most drug compounds accumulate on the surface and do not penetrate inside the nanotubes. Fig. 5-C shows drug loading using vacuum in a single step. In this image, uniform drug distribution is visible in most surface areas, preventing drug accumulation. However, due to the single-step drug loading, there are regions of nanotubes where the drug did not penetrate. It is worth mentioning that these areas contain nanotubes that do have drug content, but the excess drug has been washed off their surfaces. Finally, Fig. 5-D depicts the drug-loaded surface with uniform distribution due to multiple repetitions in the drug loading process, ensuring homogeneous drug loading throughout the surface.

In Figs. 6 and 7, EDS analysis was conducted to elucidate the presence of elements. The key bioactive compounds in garlic extract are sulfur-based compounds. Therefore, an appropriate distribution of carbon, sulfur, nitrogen, and oxygen elements on the surface suggests the potential presence of significant bioactive compounds [40,57,58]. Surface analysis was performed as depicted in Fig. 6, confirming the presence of these specified elements. Fig. 6-A shows the drug-loaded surface and 6-B indicates the percentage of elements present on the surface. The EDS mapping illustrates the elemental distribution of carbon, sulfur, nitrogen, and oxygen in Fig. 6 (C–F), respectively. Furthermore, to ensure the complete encapsulation of the drug within the nanotube pores, a side-view EDS analysis of the nanotubes was conducted, as illustrated in Fig. 7. The lateral surface of drug-loaded nanotubes is shown in Fig. 7-A. Fig. 7-B shows the composition of the nanotubes along with an EDS elemental distribution map. Fig. 7 (C–F) displays EDS elemental distribution maps, which were again used here to indicate the presence and distribution of carbon, nitrogen, oxygen, and sulfur, respectively. This analysis confirmed the distribution of specified elements observed on the upper surface of the sample (Fig. 6), providing assurance that the drug loading process was carried out effectively.

3.3. FT-IR analysis after drug loading

Following the elemental analysis using EDS to confirm the presence of vital biological constituents within the garlic extract, further validation was pursued via FT-IR analysis of the sample surface subsequent to drug loading. This step aimed to elucidate the molecular bonds present within the loaded extract, thereby verifying the presence of biologically active compounds and reconfirming the appropriate drug loading within titanium dioxide nanotubes. The resultant graph from this analysis is depicted in Fig. 8. Previous studies conducted FT-IR analysis on titanium dioxide nanotubes devoid of drug presence, revealing no discernible absorption peaks. Hence, the peaks delineated in Fig. 8 are presumably exclusively attributed to the loaded natural garlic extract within the nanotubes [48].

The prominent peak at 3267.3 cm^{-1} can be attributed to the O–H stretching of hydroxyl groups, while the peak at 2931.1 cm^{-1} corresponds to the asymmetric stretching of C–H bonds. The peak observed at 1624.3 cm^{-1} is indicative of carbonyl or carboxylic (C=O) stretching bands of peptide linkages (amides stretching). The band identified at 1408.6 cm^{-1} is associated with the -O-H bend of carboxylates. Additionally, a band at 1126.3 cm^{-1} can be ascribed to the S=O absorption of sulfones. The presence of C–N stretching vibrations in primary amines was detected at 1015.3 cm^{-1} , and at 929.7 cm^{-1} , the presence of γ -C-H deformation in =CH₂ was noted.

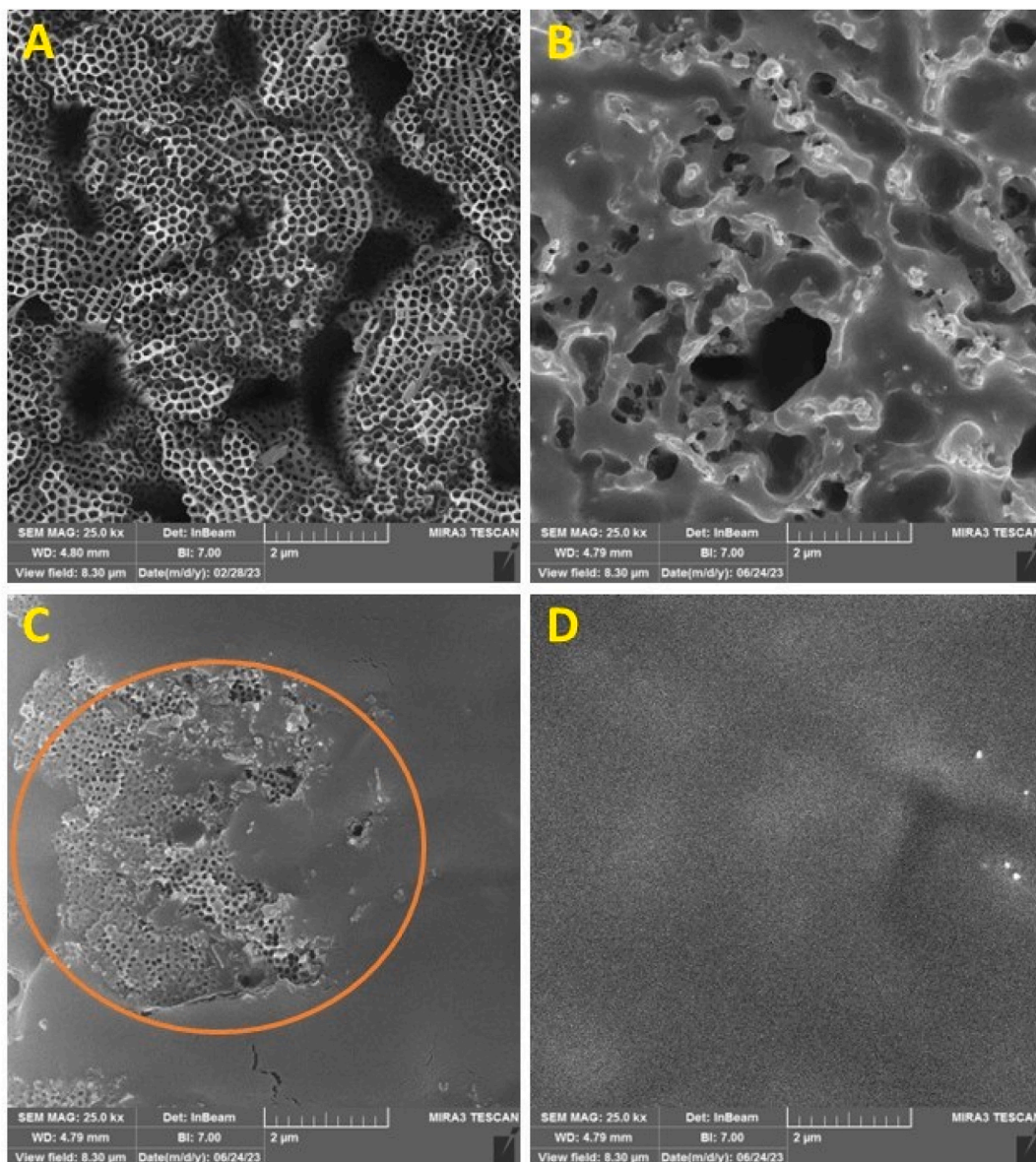


Fig. 5. FESEM images of the anodized samples before drug loading (A), after drug loading without using vacuum (B), after drug loading using vacuum (C), and drug loading using vacuum in several repetitions (D).

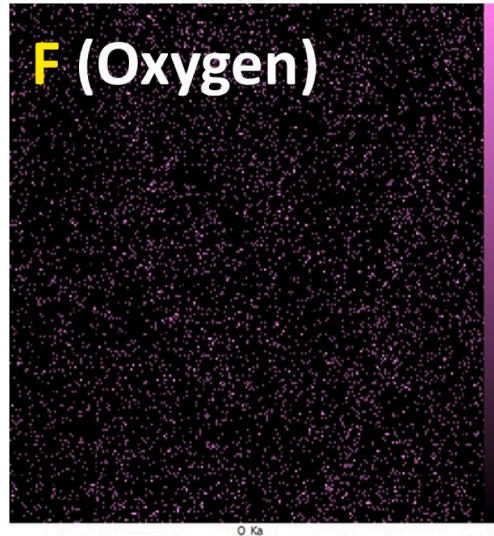
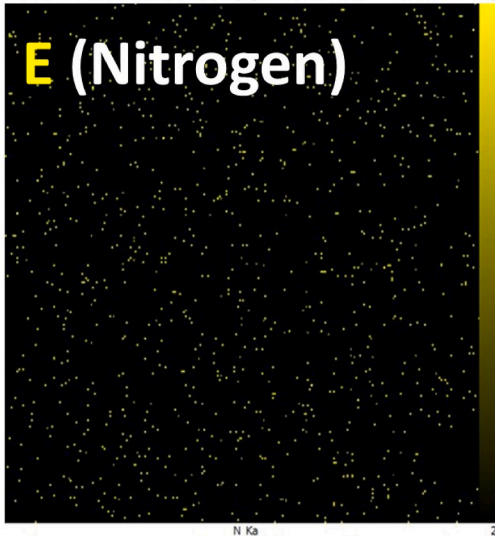
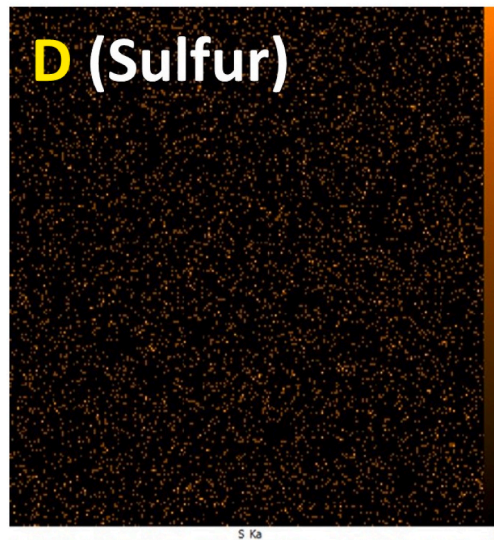
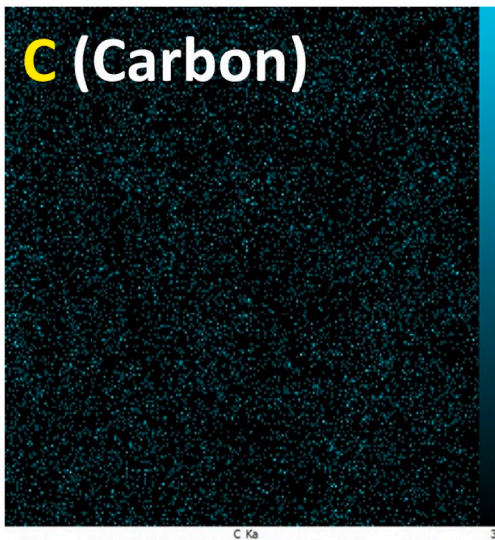
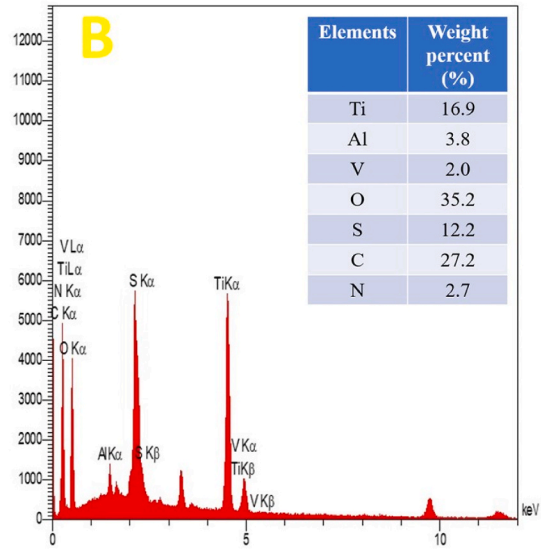
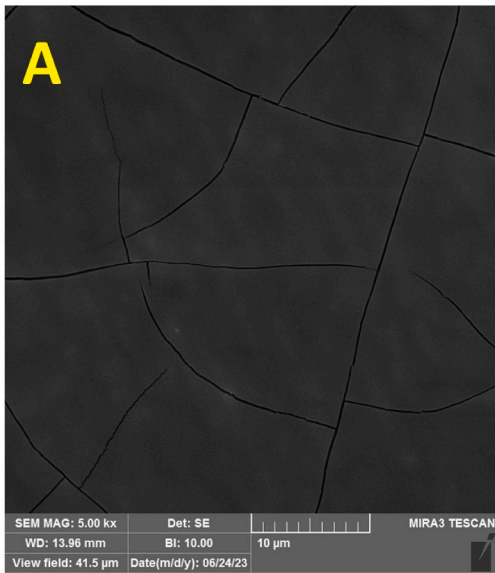
Furthermore, the presence of an S–C bond at 818.68 cm^{-1} suggests the absorption of allicin, an organosulfur compound found in garlic extract [59–65].

Based on the aforementioned spectral analysis, it can be inferred that phenolic compounds, organosulfur compounds, amino acids, carboxylic groups, and proteins constitute the active groups contributing significantly to the antibacterial activity of ultrasonicated garlic extract [66,67].

With these findings, subsequent antibacterial evaluations, cytotoxicity assessments, and cellular adhesion experiments can be conducted on the samples.

3.4. Results of the antibacterial properties of the samples

To investigate the antibacterial properties and cellular toxicity assessments, four sample groups were considered. The first group comprises the Ti6A14V alloy without any surface modifications, hereafter referred to as Group Ti64. The second group consists of the Ti6A14V alloy coated with titanium dioxide nanotubes, designated as Group Ti64+TNT. The third and fourth groups involve two variations of natural garlic extract loaded into the created nanotubes on the surface of the Ti6A14V alloy. These groups are named



(caption on next page)

Fig. 6. (A) FESEM image of the drug-loaded surface, (B) The percentage of elements present on the surface and (C–F) The EDS mapping illustrates the elemental distribution in the order of carbon, sulfur, nitrogen, and oxygen.

Ti64+TNT+0.1GAR and Ti64+TNT+0.2GAR, respectively. The results of the antibacterial experiments against *S. aureus* and *E. Coli* are presented in Fig. 9 (A–B) respectively, and Fig. 10 shows the images of the agar plates of control group, Ti64, Ti64+TNT, Ti64+TNT+0.1GAR, and Ti64+TNT+0.2GAR against *E. Coli* (A1–5) and *S. aureus* (B1–5) respectively.

The colony-forming unit (CFU) counting method was chosen for antibacterial testing. This method includes a control group in which bacteria can grow without any hindrance. By comparing the first group, which consisted of unmodified surface samples, with the control group, it can be determined whether the sample possesses intrinsic antibacterial properties. Results in Fig. 9 show that for both bacteria, the first group, Ti64, promotes bacterial growth compared to the controlled group. This implies that the Ti6A14V implant does not possess inherent antibacterial properties and even provides a suitable surface for bacterial growth. Therefore, surface modifications are crucial [68].

The second group, Ti64+TNT, formed nanotube structures on the implant's surface, as shown in Fig. 9-A, exhibited resistance against *S. aureus* bacterial growth and not only demonstrated less growth than the first group but also fewer bacteria compared to the control group. However, the number of bacteria in this group, like the control and the first group, still fell within the range of 10^9 CFU per ml. Against *E. coli* bacteria (Fig. 9-B), the second group displayed better antibacterial properties than the first group, but an increase in bacterial count was accompanied.

To examine the cause of this phenomenon, it must be noted that antibacterial mechanisms are complex, including charge repulsion, membrane adhesion, and surface roughness alteration. Charge repulsion between TNTs and bacteria prevents initial adhesion. Many bacteria have negative charges on their surfaces. For instance, major components of *S. aureus* cell wall, teichoic and lipoteichoic acids, lead to a negatively charged surface. The presence of similar charges between bacteria and TNTs creates repulsive forces, reducing bacterial adhesion. Created pull forces by TNT nanostructures cause bacterial death extension. When bacteria contact TNTs continuously, bacterial surface stretches and parts of membranes become suspended in gaps, eventually leading to bacterial rupture.

Surface roughness also plays a significant role in TNTs' antibacterial efficacy. Firstly, it might affect surface wetting. Hydrophobic surfaces tend to adhere to other hydrophobic surfaces because their hydrophilic structures tend to absorb a layer of water, which needs to be removed before hydrophilic bacterial adhesion. The high roughness of TNTs significantly increases surface hydrophilicity, preventing adhesion. Secondly, the effects of roughness on antibacterial properties are entirely different at the nano or microscale. Bacterial adhesion decreases with increased surface roughness at the nanoscale (10–100 nm).

When surface roughness enters or approaches the micron scale, bacterial adhesion increases in parallel with surface roughness. This phenomenon can be explained by the theory of contact points, which states that for organisms smaller than the tissue scale, increased roughness leads to more attachment points and creates shelters on a microscale, protecting adhesive organisms against hydrodynamic shear forces. Perhaps, this theory could justify the increase in the number of bacteria in the first group, as the sample Ti64 likely possesses surface roughness in the micron range, creating suitable sites for bacterial presence, although the contact angle and surface energy also play a role. It is essential to note that changes in dimension parameters result in torque forces, determining the antibacterial ability of TNTs. Nanotube diameter is a crucial parameter, and with increased diameter, surface roughness and hydrophilicity also increase [69,70].

Regarding the third and fourth groups containing garlic extract at different concentrations, as expected and as indicated in numerous studies [41,66,71–76] they exhibited significantly better antibacterial properties compared to the first and second groups. Confronting *S. aureus* bacteria, the third and fourth groups reduced the bacterial count from the range of 10^9 CFU/ml in the first and second groups to the range of 10^6 CFU/ml. Similarly, facing *E. coli*, the bacterial count reduced from the range of 10^{11} CFU/ml in the first and second groups to 10^9 CFU/ml.

As mentioned, the antibacterial properties of garlic extract are attributed to its sulfur-containing organic compounds. Two main mechanisms of antibacterial properties of sulfur-containing garlic compounds have been elucidated from reported studies: 1- reactions of garlic compounds with free sulfhydryl groups on proteins and/or bacterial enzymes for their inactivation and 2- disruption in bacterial cell membrane composition and integrity. Additionally, some studies also show that garlic compounds can inhibit the synthesis of DNA, RNA, and proteins in bacteria. These mechanisms are observed in both Gram-positive and Gram-negative bacteria, indicating that garlic and its compounds employ similar antibacterial mechanisms for both bacterial groups [40].

To observe the antibacterial properties rates of the groups, the data presented in Fig. 9 were converted into percentage values using Equation (2) [77]. The results against *S. aureus* and *E. Coli* are depicted in Fig. 11 (A and B) respectively.

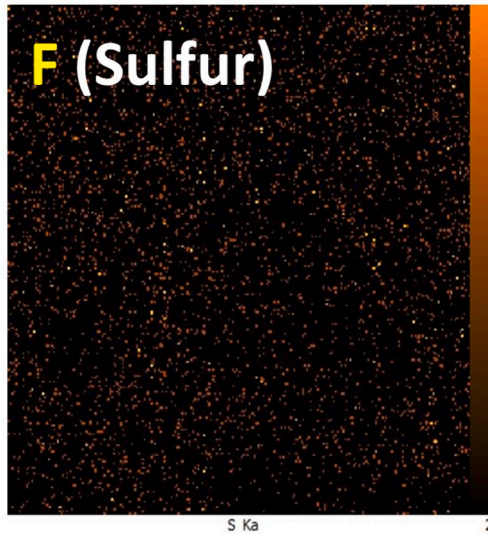
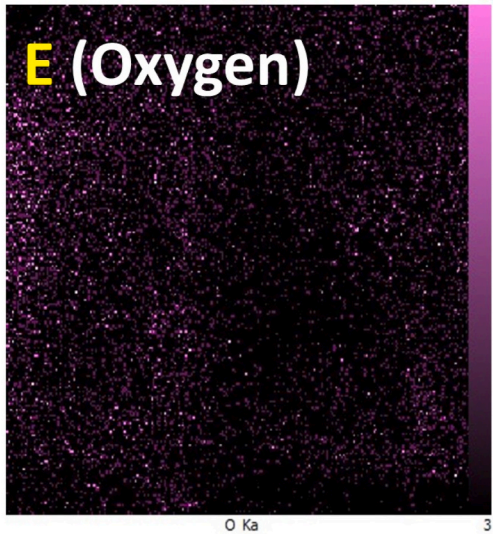
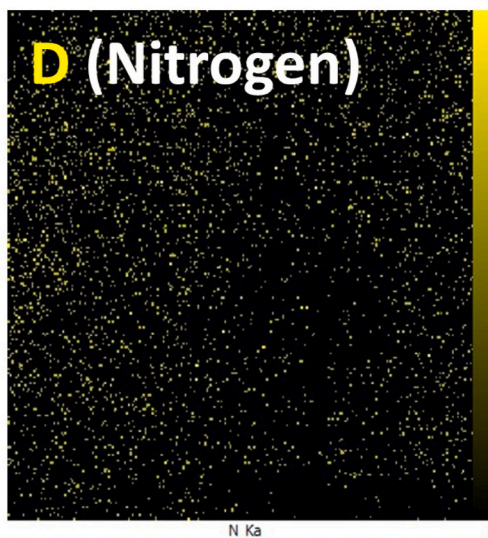
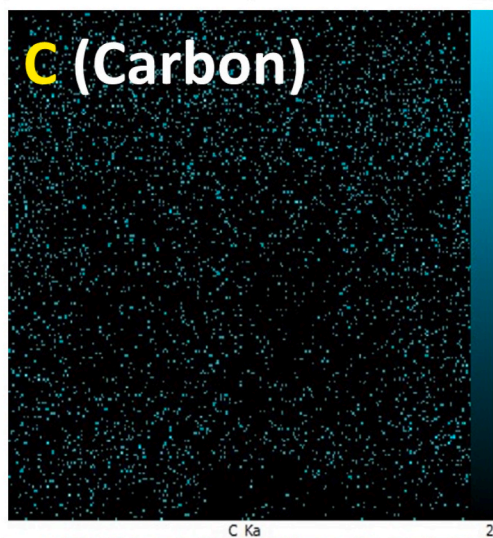
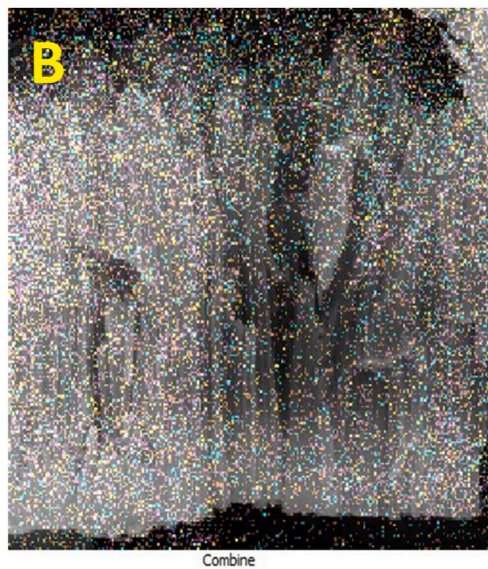
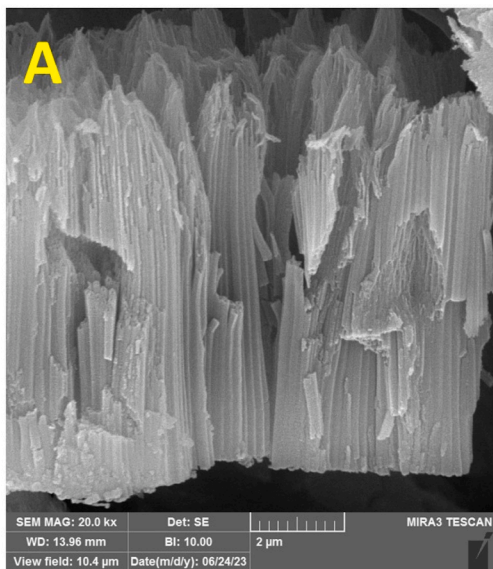
$$\text{Antibacterial rate (\%)} = \text{AR} = \left(\frac{A - B}{A} \right) \times 100 \quad \text{Equation (2)}$$

In this equation, A represents the CFU per ml value in the samples of the first group, and B represents the CFU per ml value in the samples of the specified groups. In this context, the antibacterial properties of the samples in the first group were assumed to be zero percent.

3.5. Cellular toxicity assessment

To assess cellular toxicity, as mentioned earlier, MTT assay was employed (Fig. 12).

As observed in Fig. 12, in the first group, namely Ti64, approximately 8% of cells were lost after 1 day, and around 10% were lost



(caption on next page)

Fig. 7. (A) FESEM image of the lateral surface of drug-loaded nanotubes, (B) The composition of the nanotubes along with an EDS elemental distribution map and (C–F) EDS elemental distribution maps indicating the presence and distribution of carbon, nitrogen, oxygen, and sulfur respectively.

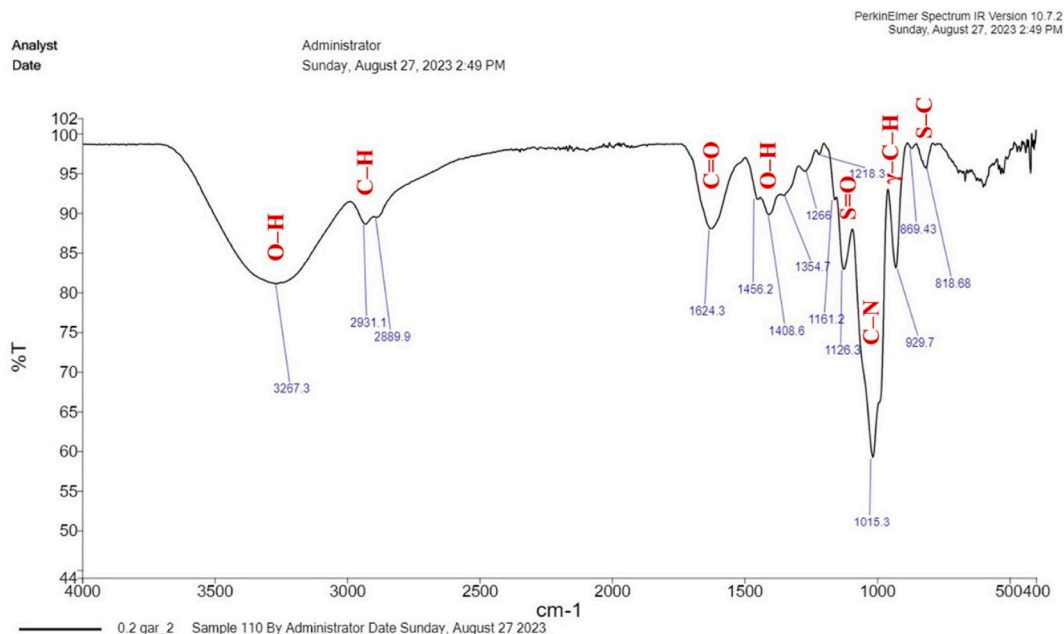


Fig. 8. The FT-IR analysis of the surface of nanotubes containing garlic extract.

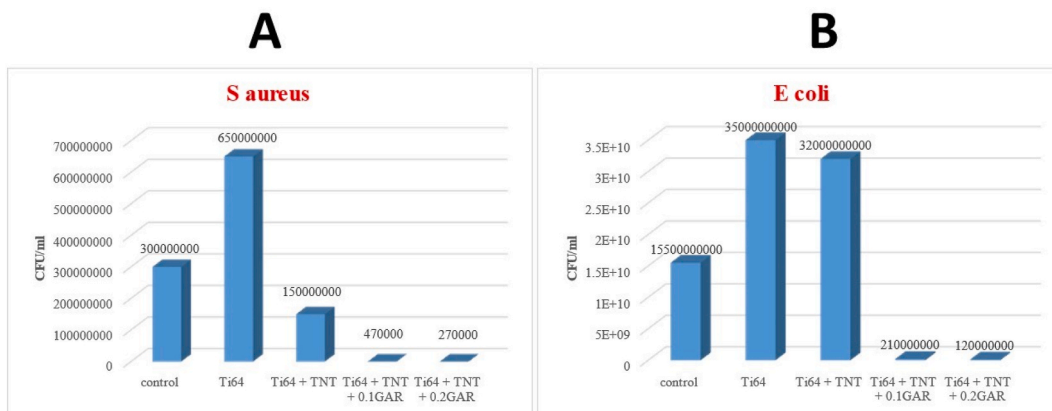


Fig. 9. Results of the colony-forming unit (CFU) assay in the face of (A) *S. aureus* and (B) *E. coli* bacteria.

after 3 days. Subsequently, in the Ti64+TNT group and Ti64+TNT+0.1GAR group, not only was the number of cells not reduced, but also approximately 3% and 8% more cells were added, respectively, after 3 days. However, a different outcome occurred in the Ti64+TNT+0.2GAR group. As observed, the number of cells in this group decreased from 100% to nearly 65% after 3 days, indicating a 35% reduction in cells and cellular toxicity (Each group underwent three repeats of analysis).

3.6. Cell adhesion

Cell adhesion images of all samples including Ti64, Ti64+TNT, Ti64+TNT+0.1GAR, and Ti64+TNT+0.2GAR captured by FESEM microscopy are presented in Fig. 13 (A–D) and 14 (A–B, C–D, E–F and G–H) respectively.

As evident in Fig. 13, cell distribution in the first and fourth groups is significantly lower compared to the second and third groups, confirming the results obtained from the MTT assay. Fig. 14 illustrates that cells in the first group appear spherical, indicating their lack

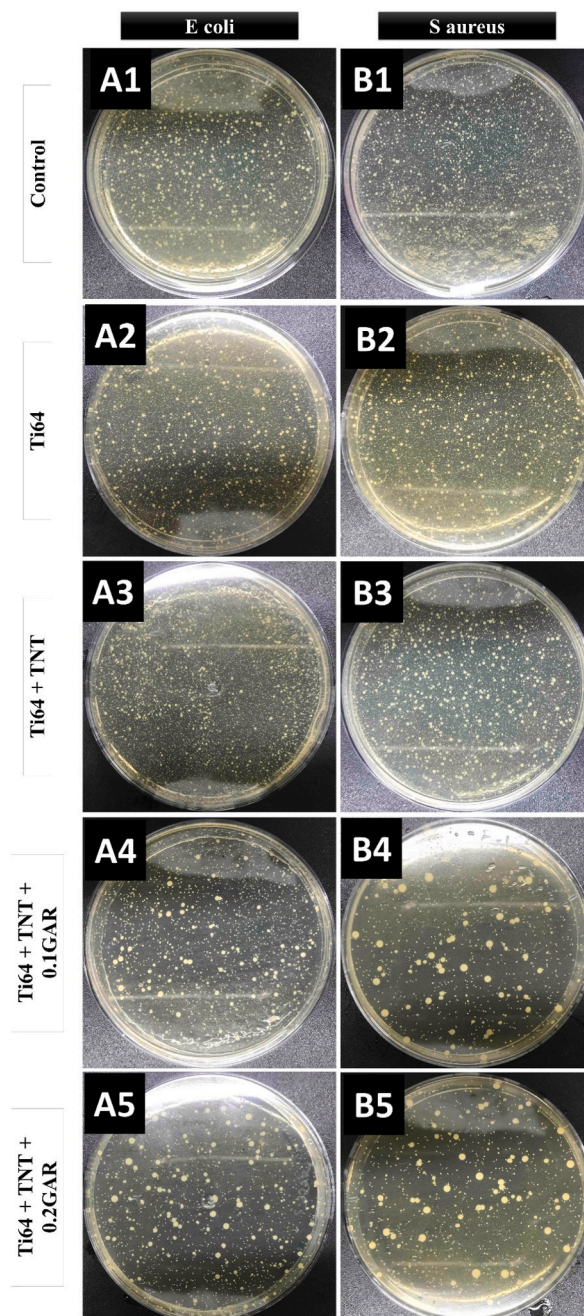


Fig. 10. The images of agar plates represent four experimental groups along with the control group, when exposed to *S. aureus* and *E. coli*.

of inclination for adhesion. In the second and third groups, cells are observed to adhere to the surface, and in the third group, they are completely settled. In these two groups, cellular filopodia extensively spread out, with the nanotube surface acting as an anchorage site. The presence of nanotubes on the surface results in proper cell adhesion due to alterations in surface roughness, wettability, and surface energy [78]. Furthermore, the uniform structure of nanotube openings can significantly alter cell behavior. Recent studies have shown that integrin activation is influenced not only by the surface chemistry of the cell-material interface but also by surface nanotopographical features, including nanotube diameter [79]. By analyzing the fourth group, it is observed that cells have reverted to a spherical state once again.

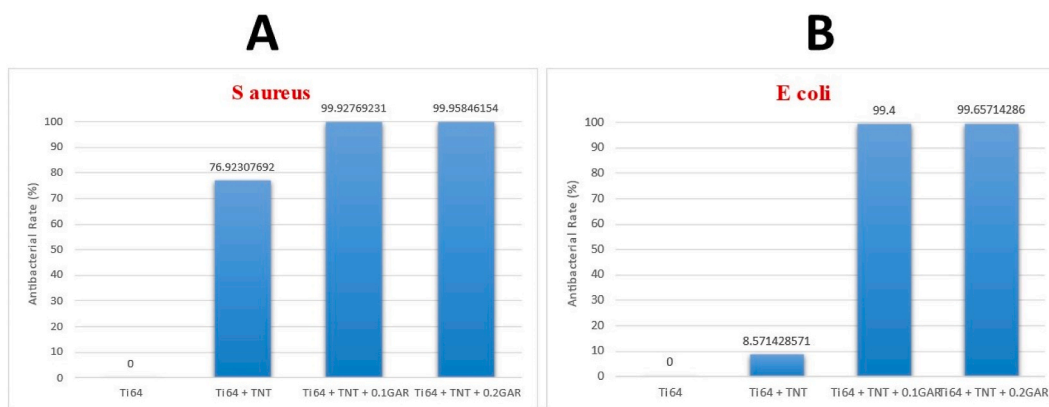


Fig. 11. The antibacterial properties of groups 1 to 4 when exposed to (A) *S. aureus* and (B) *E. coli*.

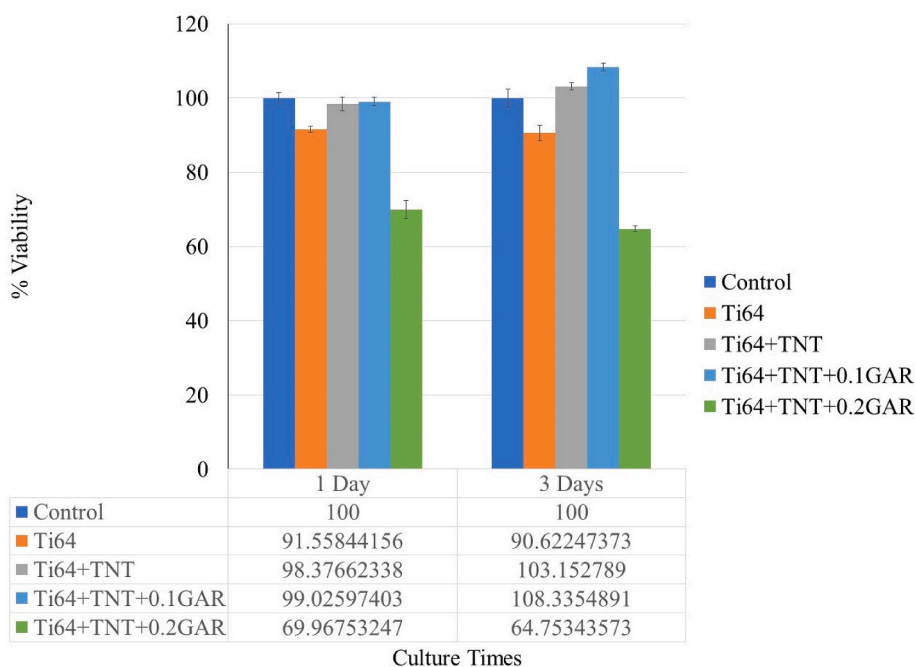


Fig. 12. MTT assay of all groups after 1 and 3 days.

3.7. Identification of compounds present in garlic extract

In light of the results obtained from the antibacterial properties, MTT assay, and cell adhesion assessments, it is imperative to identify the compounds present in the garlic extract to analyze the observed events. For this purpose, Gas Chromatography-Mass Spectrometry (GC-MS) analysis was employed. The results of this analysis are depicted in Table 1 and Fig. 15.

The compounds specified in Table 1 indicate the presence of sulfur compounds in garlic extract, responsible for its antibacterial properties (compounds 2 to 5). Compound number 7, Gibberellin A3, is responsible for cell growth and elongation in plants. Compound number 9, Heneicosane has demonstrated excellent antimicrobial activity against certain bacteria [80].

Until now, no harmful activity has been reported in relation to the mentioned compounds. However, concerning compound number 6, diethyl phthalate, various discussions have been ongoing in the literature. Phthalates are a group of widely used chemical substances indicating endocrine disruptions and posing health hazards to humans. Despite their short half-life in tissues, chronic exposure to phthalates adversely affects the endocrine system and the functioning of multiple organs, exerting long-term negative effects on fertility, growth, and development in children and the reproductive system in children and adolescents.

Phthalic acid esters (PAEs) are common plasticizers added to polymer materials to enhance their flexibility and performance. To date, most published articles have focused on detection methods, distribution of contamination, and toxicological hazards of PAEs. However, natural sources of various PAEs are rarely studied. The first reports of phthalic acid as a natural substance were published in

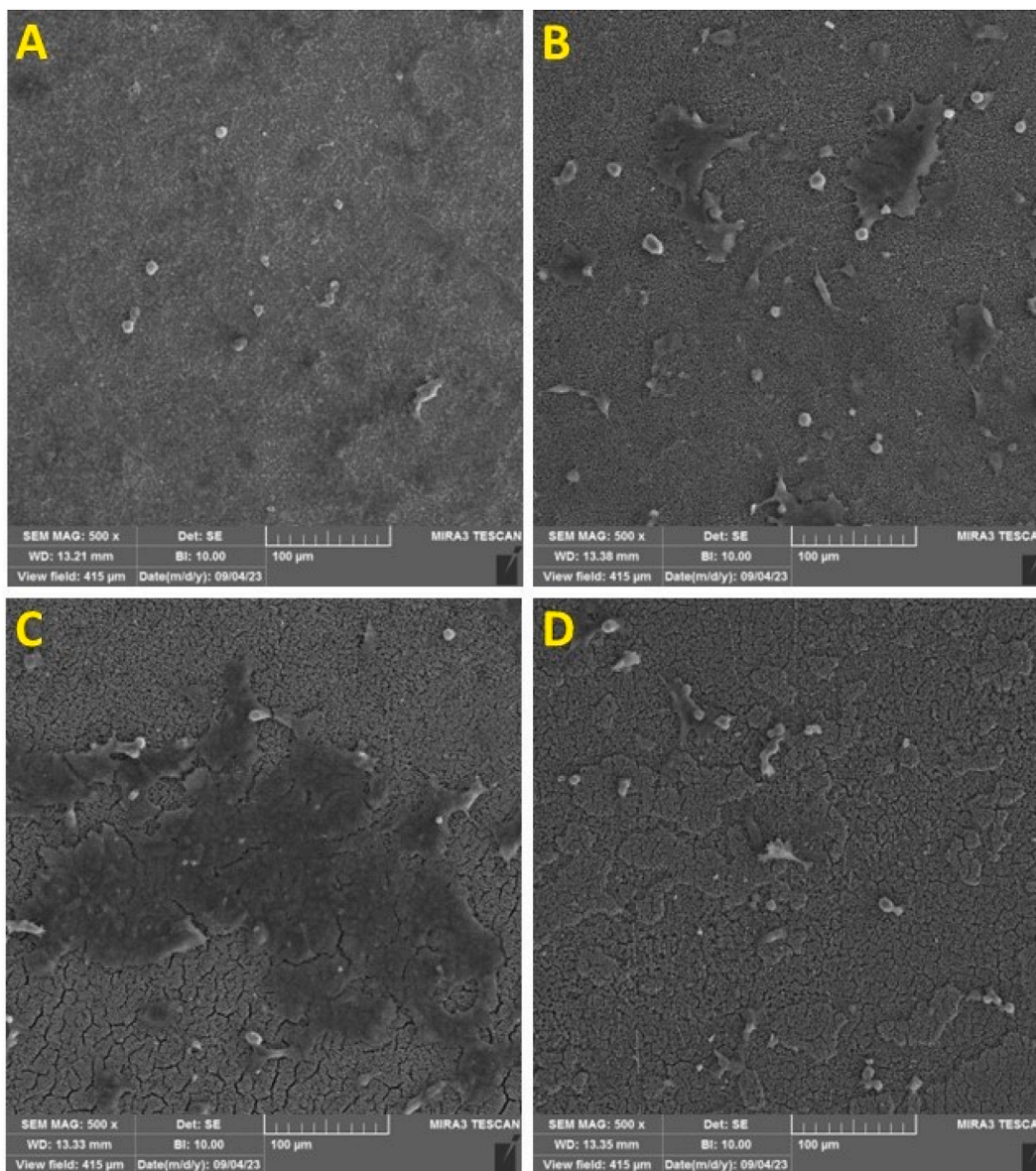


Fig. 13. FESEM images indicate the distribution of MG63 cells on the surfaces of the samples. (A) Ti64, (B) Ti64+TNT, (C) Ti64+TNT+0.1GAR, (D) Ti64+TNT+0.2GAR.

1945, and since then, over 50 different derivatives of PAEs from various classification groups, including bacteria, actinomycetes, fungi, higher plants, and even animals, have been reported. However, what remains unclear is whether these compounds are synthetically derived substances that later contribute to air, water, or soil pollution or if they may be produced by plants and microorganisms themselves. PAEs have been identified in organic extracts of specific plant species via GC-MS, with their percentage ranging from 0.10% to 0.32%. Most PAEs were found in plant essences, indicating that identified and purified PAEs in plant materials suggest that plants may synthesize them to some extent. Synthetic PAEs entering the ecosystem may disrupt the metabolic processes of some plant, algal, and microbial communities. Therefore, further studies are needed to elucidate the relevant mechanisms and ecological consequences [81,82].

Given the aforementioned information, it is possible that the toxicity induced by samples from the fourth group, namely Ti64+TNT+0.2GAR, which contain a higher dose of garlic extract, could be due to the increased presence of phthalate-related compounds. These compounds might damage the cell membrane of MG63 cells. However, further research is necessary to clarify this discussion conclusively.

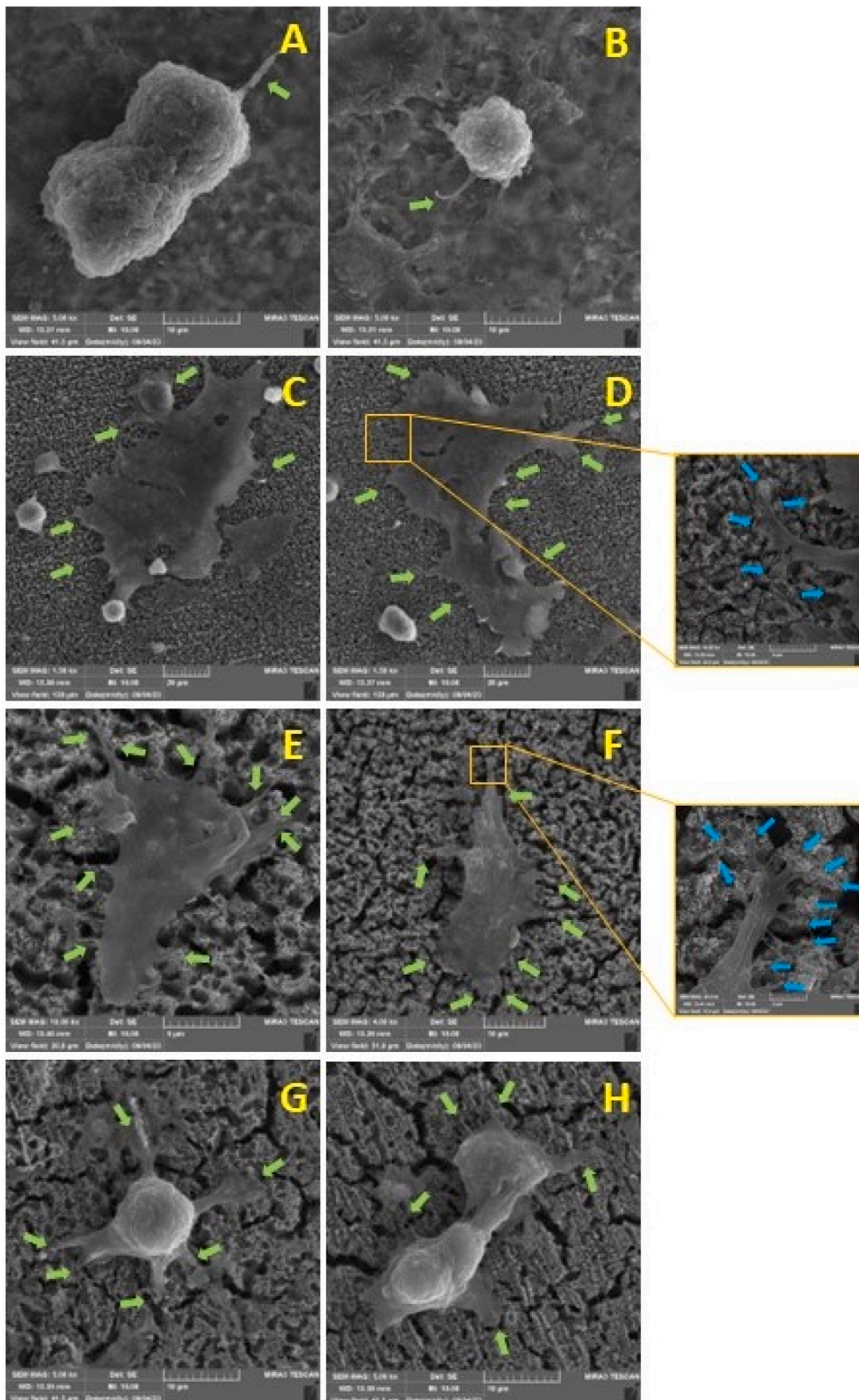


Fig. 14. FESEM images indicating the adhesion of MG63 cells onto the surfaces of the samples: Ti64 (A, B), Ti64+TNT accompanied by a magnified view of cellular filopodia (C, D), Ti64+TNT+0.1GAR along with an enlarged view of cellular filopodia (E, F), and Ti64+TNT+0.2GAR (G, H).

Table 1
Existing compounds in garlic extract.

No	RT (min)	Area (Ab*s)	Area%	Name	Quality
1	5.638	11328944	8.05	Silane, trimethyl(phenethylthio)-	14
2	8.72	2889667	2.05	Diallyl disulphide	27
3	9.244	3206778	2.28	Disulfide, (1E)-1-propen-1-yl 2-propen-1-yl	49
4	11.097	39327942	27.94	3-Vinyl-1,2-dithia-5-cyclohexene	98
5	11.59	19586055	13.92	3-Vinyl-1,2-dithiocyclohex-5-ene	96
6	19.689	7185605	5.11	Diethyl phthalate	97
7	50.255	4823262	3.43	Gibberellin A3	38
8	46.276	37651097	26.75	Alkanox 240	78
9	26.471	2682818	1.91	Heneicosane	91
10	32.417	2130796	1.51	Mandelic acid	47

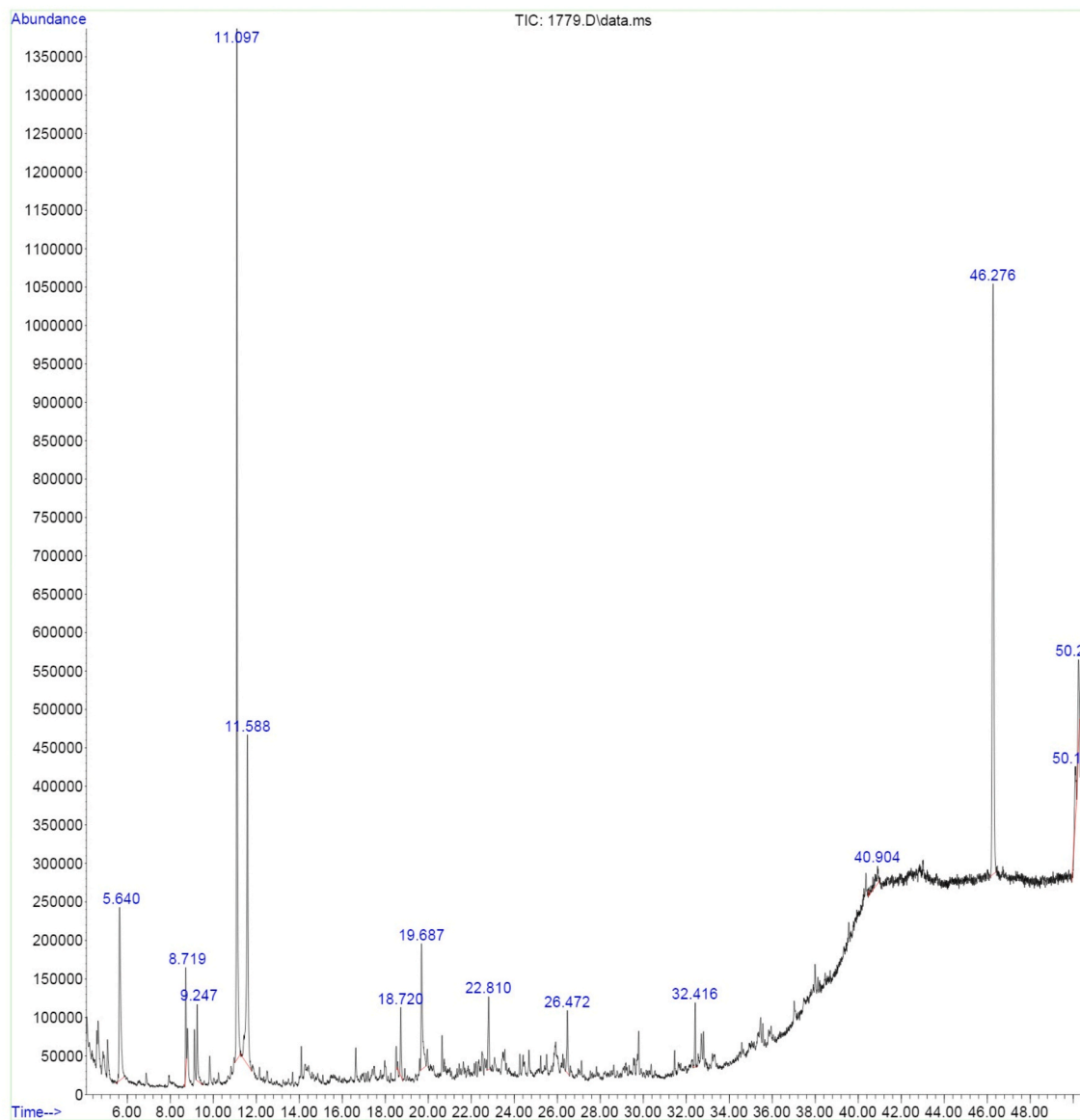


Fig. 15. The GC-MS analysis graph of the prepared garlic extract.

4. Conclusion

Orthopedic implants are widely used in bone replacement surgeries nowadays. Ongoing efforts are focused on developing these implants, with one such endeavor involving the utilization of various surface modification strategies to combat infections and toxicities, which are primary reasons for implant failure and associated complications. Targeted drug delivery systems implemented through modified implants have the potential to fulfill many expectations and essential prerequisites for successful implantation. The use of nanoparticles loaded with therapeutic agents presents a promising alternative for the development of localized drug delivery systems, capable of overcoming limitations associated with systemic drug therapies.

In the present study, to enhance the antibacterial properties of Ti6Al4V implants and address the issue of bacteria resistant to antibiotics, a natural herbal extract of garlic loaded into titanium oxide nanotubes was employed. Laboratory investigations demonstrated that nanotubes containing an appropriate concentration of garlic extract (0.1 g per milliliter) not only exhibited over 99% antibacterial activity against Gram-positive *Staphylococcus aureus* and Gram-negative *Escherichia coli* but also showed no adverse effects on MG63 cells, with an observed 8% increase in cell proliferation. Furthermore, it was observed that nanotubes without drug loading also possessed moderate antibacterial properties. Conversely, samples containing higher concentrations of the extract (0.2 g per milliliter) resulted in toxicity, causing a 35% reduction in cell viability. Gas chromatography-mass spectrometry (GC-MS) analysis, in addition to identifying sulfur compounds responsible for the antibacterial properties of garlic, revealed the presence of diethyl phthalates. The presence of such compounds, sometimes found in synthetically produced substances and whose origin in certain plants is still debated, may contribute to cellular toxicity.

The presence of numerous and diverse compounds in herbal extracts has posed challenges in working with these materials. Therefore, further investigations are imperative to optimize extraction methods, preserve beneficial compounds, eliminate harmful ones, and evaluate the synergistic effects of different herbal extracts to enhance the properties of natural drugs. Considering that some harmful compounds may infiltrate plants due to environmental contamination from chemical waste, the assessment and preservation of plant cultivation environments' health should also be considered.

Ultimately, with promising results obtained from samples containing appropriate doses of herbal extracts, there is hope that the issue of microbial resistance can be addressed through the use of herbal therapeutic compounds. However, achieving this goal undoubtedly necessitates a deep understanding of the functional mechanisms of herbal compounds in interacting with microorganisms and living cells, as well as further research and experimentation in this field.

Data availability statement

Data will be made available on request.

CRediT authorship contribution statement

Sadegh Jafari Jebeli: Conceptualization. **Rouhollah Mehdiavaz Aghdam:** Supervision. **Aryan Najjari:** Writing – review & editing. **Reza Soltani:** Writing – review & editing.

Declaration of competing interest

The authors declare that they have no known competing financial interests or personal relationships that could have appeared to influence the work reported in this paper.

References

- [1] N. Jiang, et al., "Promoting osseointegration of Ti implants through micro/nanoscaled hierarchical Ti phosphate/Ti oxide hybrid coating, *ACS Nano* 12 (8) (2018) 7883–7891, <https://doi.org/10.1021/acsnano.8b02227>.
- [2] M. Schimmel, F. Müller, V. Suter, D. Buser, "Implants for elderly patients," *Periodontology* 2000, Blackwell Munksgaard 73 (no. 1) (2017) 228–240, <https://doi.org/10.1111/prd.12166>.
- [3] H. Lin, J. Sohn, H. Shen, M.T. Langhans, R.S. Tuan, "Bone marrow mesenchymal stem cells: aging and tissue engineering applications to enhance bone healing," *Biomaterials*, 203 (May 2019) 96–110, <https://doi.org/10.1016/j.biomaterials.2018.06.026>.
- [4] K. Ahmad, S.R. Rajpoot, H. ur R, Shah, M. Ashfaq, and Z. Ahmad, "assessment of nutritional status of undergraduate students of the islamia university Bahawalpur," in emerging trends in disease and health research, Book Publisher International (a part of SCIEENCEDOMAIN International) 1 (2021) 32–43, <https://doi.org/10.9734/bpi/etdhr/v1/15015d>.
- [5] Y. Yang, et al., "Mg bone implant: features, developments and perspectives," *Materials and Design*, Elsevier 185 (2020), <https://doi.org/10.1016/j.matdes.2019.108259>.
- [6] K. Wang, H. Jin, Q. Song, J. Huo, J. Zhang, P. Li, "Titanium dioxide nanotubes as drug carriers for infection control and osteogenesis of bone implants, *Drug Deliv Transl Res* 11 (4) (2021) 1456–1474, <https://doi.org/10.1007/s13346-021-00980-z>.
- [7] K.A. Kravanja, M. Finšgar, "A Review of Techniques for the Application of Bioactive Coatings on Metal-Based Implants to Achieve Controlled Release of Active Ingredients," *Materials and Design*, vol. 217, Elsevier Ltd, 2022, <https://doi.org/10.1016/j.matdes.2022.110653>.
- [8] J. Zan, et al., "Dilemma and breakthrough of biodegradable poly-L-lactic acid in bone tissue repair, *J. Mater. Res. Technol.* 17 (2022) 2369–2387, <https://doi.org/10.1016/j.jmrt.2022.01.164>. Elsevier Editora Ltda.
- [9] K. Budak, O. Sogut, and U. A. Sezer, "A review on synthesis and biomedical applications of polyglycolic acid", doi:10.1007/s10965-020-02187-1/Published..
- [10] L. Sbricoli, R. Guazzo, M. Annunziata, L. Gobatto, E. Bressan, L. Nastro, "Selection of collagen membranes for bone regeneration: a literature review, *Materials* 13 (no. 3) (2020), <https://doi.org/10.3390/ma13030786>.
- [11] G.A. Rico-Llanos, S. Borrego-González, M. Moncayo-Donoso, J. Becerra, R. Visser, "Collagen type I biomaterials as scaffolds for bone tissue engineering, *Polymers* 13 (4) (2021) 1–20, <https://doi.org/10.3390/polym13040599>. Basel.

- [12] A. Najjari, et al., "Smart piezoelectric biomaterials for tissue engineering and regenerative medicine: a review, *Biomedical Engineering/Biomed. Tech.* 67 (2) (2022) 71–88, <https://doi.org/10.1515/bmt-2021-0265>.
- [13] O.A. Osuchukwu, A. Salihi, I. Abdullahi, B. Abdulkareem, C.S. Nwannenna, "Synthesis techniques, characterization and mechanical properties of natural derived hydroxyapatite scaffolds for bone implants: a review, *SN Appl. Sci.* 3 (no. 10) (2021), <https://doi.org/10.1007/s42452-021-04795-y>. Springer Nature.
- [14] A.A. Vu, D.A. Burke, A. Bandyopadhyay, S. Bose, "Effects of surface area and topography on 3D printed tricalcium phosphate scaffolds for bone grafting applications, *Addit. Manuf.* 39 (2021), <https://doi.org/10.1016/j.addma.2021.101870>.
- [15] M. Bohner, B.L.G. Santoni, N. Döbelin, "β-tricalcium phosphate for bone substitution: synthesis and properties," *Acta Biomaterialia*, *Acta Mater.* 113 (2020) 23–41, <https://doi.org/10.1016/j.actbio.2020.06.022>.
- [16] S. Tangri, et al., Drug loaded bioglass nanoparticles and their coating for efficient tissue and bone regeneration, *J. Non-Cryst. Solids* 616 (2023), <https://doi.org/10.1016/j.jnoncrysol.2023.122469>. Elsevier B.V.
- [17] M. Singh, A.S. Gill, P.K. Deol, A. Agrawal, S.S. Sidhu, "Drug eluting titanium implants for localised drug delivery," *Journal of Materials Research*, Springer Nature 37 (no. 16) (2022) 2491–2511, <https://doi.org/10.1557/s43578-022-00609-y>.
- [18] J. Andrade del Olmo, et al., "Effectiveness of physicochemical techniques on the activation of Ti6Al4V surface with improved biocompatibility and antibacterial properties, *Surf. Coat. Technol.* 447 (2022), <https://doi.org/10.1016/j.surfcoat.2022.128821>.
- [19] L. Romero-Resendiz, et al., "Microstructural, mechanical, electrochemical, and biological studies of an electron beam melted Ti-6Al-4V alloy, *Mater. Today Commun.* 31 (2022), <https://doi.org/10.1016/j.mtcomm.2022.103337>.
- [20] B.C. Costa, C.K. Tokuhara, L.A. Rocha, R.C. Oliveira, P.N. Lisboa-Filho, J. Costa Pessoa, "Vanadium ionic species from degradation of Ti-6Al-4V metallic implants: in vitro cytotoxicity and speciation evaluation," *Materials Science and Engineering C*, 96 (2019) 730–739, <https://doi.org/10.1016/j.msec.2018.11.090>.
- [21] V.K. Manivasagam, R.M. Sabino, P. Kantam, K.C. Popat, "Surface modification strategies to improve titanium hemocompatibility: a comprehensive review, *Materials Advances* 2 (no. 18) (2021) 5824–5842, <https://doi.org/10.1039/d1ma00367d>. Royal Society of Chemistry.
- [22] J. Li, et al., "Combined infection control and enhanced osteogenic differentiation capacity on additive manufactured Ti-6Al-4V are mediated via titania nanotube delivery of novel biofilm inhibitors, *Adv Mater Interfaces* 7 (no. 7) (2020), <https://doi.org/10.1002/admi.201901963>.
- [23] C.R. Arciola, D. Campoccia, L. Montanaro, "Implant infections: adhesion, biofilm formation and immune evasion," *Nature Reviews Microbiology*, Nature Publishing Group 16 (no. 7) (2018) 397–409, <https://doi.org/10.1038/s41579-018-0019-y>.
- [24] T. Ji, D.S. Kohane, "Nanoscale Systems for Local Drug Delivery," *Nano Today*, vol. 28, Elsevier B.V., 2019, <https://doi.org/10.1016/j.nantod.2019.100765>.
- [25] N.J. Hickok, I.M. Shapiro, "Immobilized antibiotics to prevent orthopaedic implant infections, *Adv. Drug Deliv. Rev.* 64 (12) (2012) 1165–1176, <https://doi.org/10.1016/j.addr.2012.03.015>.
- [26] H.M. Asif, et al., "Synthesis, characterization and evaluation of anti-arthritis and anti-inflammatory potential of curcumin loaded chitosan nanoparticles, *Sci. Rep.* 13 (no. 1) (2023), <https://doi.org/10.1038/s41598-023-37152-7>.
- [27] P. Wu, D.W. Grainger, "Drug/device combinations for local drug therapies and infection prophylaxis, *Biomaterials* 27 (11) (2006) 2450–2467, <https://doi.org/10.1016/j.biomaterials.2005.11.031>.
- [28] K. Ahmad, et al., "Engineering of Zirconium based metal-organic frameworks (Zr-MOFs) as efficient adsorbents, *Mater. Sci. Eng., B* 262 (2020), <https://doi.org/10.1016/j.mseb.2020.114766>. Elsevier Ltd.
- [29] K. Huo, B. Gao, J. Fu, L. Zhao, P.K. Chu, "Fabrication, modification, and biomedical applications of anodized TiO₂ nanotube arrays, *RSC Adv.* 4 (no. 33) (2014) 17300–17324, <https://doi.org/10.1039/c4ra01458h>. Royal Society of Chemistry.
- [30] W.F. Oliveira, I.R.S. Arruda, G.M.M. Silva, G. Machado, L.C.B.B. Coelho, M.T.S. Correia, "Functionalization of Titanium Dioxide Nanotubes with Biomolecules for Biomedical Applications," *Materials Science and Engineering C*, vol. 81, Elsevier Ltd, 2017, pp. 597–606, <https://doi.org/10.1016/j.msec.2017.08.017>.
- [31] X. Ma, et al., "Titanium implants and local drug delivery systems become mutual promoters in orthopedic clinics, *Nanomaterials* 12 (no. 1) (2022), <https://doi.org/10.3390/nano12010047>. MDPI.
- [32] F. Meng, Z. Yin, X. Ren, Z. Geng, J. Su, "Construction of local drug delivery system on titanium-based implants to improve osseointegration, *Pharmaceutics* 14 (no. 5) (2022), <https://doi.org/10.3390/pharmaceutics14051069>. MDPI.
- [33] E. Feng, et al., "Improved osteogenic activity and inhibited bacterial biofilm formation on andrographolide-loaded titania nanotubes, *Ann. Transl. Med.* 8 (16) (2020), <https://doi.org/10.21037/atm-20-4901>, 987–987.
- [34] K.A. Khalil Ahmad, et al., "Synthesis of new series of phenyl diazene based metal complexes for designing most active antibacterial and antifungal agents, *J. Chem. Soc. Pakistan* 43 (5) (2021), <https://doi.org/10.52568/000599/jcsp/43.05.2021>, 578–578.
- [35] H. Hafsa, U.R. Shah, K. Ahmad, M. Ashfaq, H. Oku, "Free radical scavenging, antibacterial potentials and spectroscopic characterizations of benzoyl thiourea derivatives and their metal complexes," *J. Mol. Struct.* (2023) <https://doi.org/10.1016/j.molstruc.2022.134162>.
- [36] S. Parveen, et al., "Design, synthesis and spectroscopic characterizations of medicinal hydrazide derivatives and metal complexes of malonic ester, *Curr. Bioact. Compd.* 19 (no. 4) (May 2023), <https://doi.org/10.2174/1573407218666211222124947>.
- [37] X. Huang, et al., "Biological synthesis of bimetallic hybrid nanocomposite: a remarkable photocatalyst, adsorption/desorption and antimicrobial agent, *Applied Surface Science Advances* 17 (2023), <https://doi.org/10.1016/j.apsadv.2023.100446>.
- [38] P. Guglielmi, V. Pontecorvi, G. Rotondi, "Natural compounds and extracts as novel antimicrobial agents, *Expert Opin. Ther. Pat.* 30 (no. 12) (2020) 949–962, <https://doi.org/10.1080/13543776.2020.1853101>. Taylor and Francis Ltd.
- [39] S. Bose, N. Sarkar, D. Banerjee, "Natural medicine delivery from biomedical devices to treat bone disorders: a review," *Acta Biomaterialia*, *Acta Mater.* 126 (2021) 63–91, <https://doi.org/10.1016/j.actbio.2021.02.034>.
- [40] S.B. Bhatwalkar, R. Mondal, S.B.N. Krishna, J.K. Adam, P. Govender, R. Anupam, "Antibacterial properties of organosulfur compounds of garlic (*Allium sativum*)," *Frontiers in Microbiology*, *Frontiers Media S.A.* 12 (2021), <https://doi.org/10.3389/fmicb.2021.613077>.
- [41] W. T, K. H, T. K, Y. A, "Anti-bacterial activity of garlic extract against human pathogenic bacteria, *J Pharmacovigil* 6 (no. 01) (2018), <https://doi.org/10.4172/2329-6887.1000253>.
- [42] X.Y. Zhu, Y.R. Zeng, "Garlic extract in prosthesis-related infections: a literature review, *J. Int. Med. Res.* 48 (no. 4) (2020), <https://doi.org/10.1177/0300060520913778>. SAGE Publications Ltd.
- [43] B.T. Nguyen, H.T. Hong, T.J. O'Hare, J.B. Wehr, N.W. Menzies, S.M. Harper, "A rapid and simplified methodology for the extraction and quantification of allicin in garlic, *J. Food Compos. Anal.* 104 (2021), <https://doi.org/10.1016/j.jfca.2021.104114>.
- [44] C.M.B. Pinilla, C.P.Z. Noreña, A. Brandelli, "Development and characterization of phosphatidylcholine nanovesicles, containing garlic extract, with antilisterial activity in milk, *Food Chem.* 220 (2017) 470–476, <https://doi.org/10.1016/j.foodchem.2016.10.027>.
- [45] H. Fujisawa, K. Suma, K. Origuchi, T. Seki, T. Ariga, "Thermostability of allicin determined by chemical and biological assays, *Biosci. Biotechnol. Biochem.* 72 (11) (2008) 2877–2883, <https://doi.org/10.1271/bbb.80381>.
- [46] A. Goudarzi, S.K. Sadmezhhaad, N. Johari, "The prominent role of fully-controlled surface co-modification procedure using titanium nanotubes and silk fibroin nanofibers in the performance enhancement of Ti6Al4V implants, *Surf. Coat. Technol.* 412 (2021), <https://doi.org/10.1016/j.surfcoat.2021.127001>.
- [47] X. Niu, L. Sun, X. Zhang, Y. Sun, J. Wang, "Fabrication and antibacterial properties of cefuroxime-loaded TiO₂ nanotubes, *Appl. Microbiol. Biotechnol.* 104 (7) (2020) 2947–2955, <https://doi.org/10.1007/s00253-020-10446-w>.
- [48] H. Jia, L.L. Kerr, "Kinetics of drug release from drug carrier of polymer/TiO₂ nanotubes composite - PH dependent study, *J. Appl. Polym. Sci.* 132 (no. 7) (2015), <https://doi.org/10.1002/app.41570>.
- [49] S. Kamiloglu, G. Sari, T. Ozdal, E. Capanoglu, "Guidelines for cell viability assays, *Food Front* 1 (3) (2020) 332–349, <https://doi.org/10.1002/fft.2.44>.
- [50] D. Decha-umphai, et al., "Effects of post-processing on microstructure and adhesion strength of TiO₂ nanotubes on 3D-printed Ti-6Al-4V alloy, *Surf. Coat. Technol.* 421 (2021) 127431, <https://doi.org/10.1016/j.surfcoat.2021.127431>.
- [51] B. Ribeiro, R. Offoiaich, E. Rahimi, E. Salatin, M. Lekka, L. Fedrizzi, "On growth and morphology of tio₂ nanotubes on ti6al4v by anodic oxidation in ethylene glycol electrolyte: influence of microstructure and anodization parameters, *Materials* 14 (no. 10) (May 2021), <https://doi.org/10.3390/ma14102540>.

- [52] A. Radtke, et al., "The bioactivity and photocatalytic properties of titania nanotube coatings produced with the use of the low-potential anodization of Ti6Al4V alloy surface, *Nanomaterials* 7 (no. 8) (2017), <https://doi.org/10.3390/nano7080197>.
- [53] D. Khudhair, et al., "Anodization parameters influencing the morphology and electrical properties of TiO₂ nanotubes for living cell interfacing and investigations, *Mater. Sci. Eng. C* 59 (2016) 1125–1142, <https://doi.org/10.1016/j.msec.2015.10.042>. Elsevier Ltd.
- [54] T. Theivasanthi and M. Alagar, Titanium Dioxide (TiO₂) Nanoparticles-XRD Analyses-An Insight. .
- [55] P. Praveen, G. Viruthagiri, S. Mugundan, N. Shanmugam, "Structural, optical and morphological analyses of pristine titanium di-oxide nanoparticles - synthesized via sol-gel route, *Spectrochim. Acta Mol. Biomol. Spectrosc.* 117 (2014) 622–629, <https://doi.org/10.1016/j.saa.2013.09.037>.
- [56] L. Tang, J. Fan, H. Kou, B. Tang, J. Li, L. Tang, et al., Effect of oxygen variation on high cycle fatigue behavior of Ti-6Al-4V titanium alloy. (*Materials* 2020, 13, 3858), *Materials* 13 (no. 23) (2020) 1–2, <https://doi.org/10.3390/ma13235364>. MDPI AG.
- [57] A. Shang, et al., "Bioactive compounds and biological functions of garlic (*Allium sativum* L.), *Foods* 8 (no. 7) (2019), <https://doi.org/10.3390/foods8070246>. MDPI Multidisciplinary Digital Publishing Institute.
- [58] L. Melguizo-Rodríguez, E. García-Recio, C. Ruiz, E. De Luna-Bertos, R. Illescas-Montes, V.J. Costela-Ruiz, "Biological properties and therapeutic applications of garlic and its components, *Food Funct.* 13 (no. 5) (2022) 2415–2426, <https://doi.org/10.1039/d1fo03180e>. Royal Society of Chemistry.
- [59] Y. Yulizar, A. Ariyanta, L. Abdurrachman, "Green Synthesis of Goccoparticles using Aqueous Garlic (*Allium sativum* L.) Extract and Its Interaction Study with Melamine," (2017), <https://doi.org/10.9767/bcrec.12.2.770.212>.
- [60] L. Rastogi, J. Arunachalam, "Sunlight based irradiation strategy for rapid green synthesis of highly stable silver nanoparticles using aqueous garlic (*Allium sativum*) extract and their antibacterial potential, *Mater. Chem. Phys.* 129 (no. 1–2) (2011) 558–563, <https://doi.org/10.1016/j.matchemphys.2011.04.068>.
- [61] B.J. Divya, B. Suman, M. Venkataswamy, K. Thyagaraju, "A STUDY ON PHYTOCHEMICALS, FUNCTIONAL GROUPS AND MINERAL COMPOSITION OF ALLIUM SATIVUM (GARLIC) CLOVES," (2017), <https://doi.org/10.22159/ijcpr.2017v9i3.18888>.
- [62] X. Lu, B.A. Rasco, J.M.F. Jabal, D. Eric Aston, M. Lin, M.E. Konkel, "Investigating antibacterial effects of garlic (*Allium sativum*) concentrate and garlic-derived organosulfur compounds on *Campylobacter jejuni* by using fourier transform infrared spectroscopy, Raman spectroscopy, and electron microscopy, *Appl. Environ. Microbiol.* 77 (15) (2011) 5257–5269, <https://doi.org/10.1128/AEM.02845-10>.
- [63] K. Rajam, S. Rajendran, R. Saranya, "Allium sativum (Garlic) extract as nontoxic corrosion inhibitor, *J. Chem.* (2013), <https://doi.org/10.1155/2013/743807>.
- [64] A.B.D. Nandiyanto, R. Oktiani, R. Ragadhita, "How to read and interpret ftr spectroscopy of organic material, *Indonesian Journal of Science and Technology* 4 (1) (2019) 97–118, <https://doi.org/10.17509/ijost.v4i1.15806>.
- [65] L. Rastogi, J. Arunachalam, "Green synthesis route for the size controlled synthesis of biocompatible gold nanoparticles using aqueous extract of garlic (*Allium sativum*), *Adv. Mater. Lett.* 4 (7) (2013) 548–555, <https://doi.org/10.5185/amlett.2012.11456>.
- [66] T. Gabriel, A. Vestire, K.D. Kim, S.J. Kwon, I. Sivanesan, S.C. Chun, "Antibacterial activity of nanoparticles of garlic (*Allium sativum*) extract against different bacteria such as *Streptococcus mutans* and *Porphomonas gingivalis*, *Appl. Sci.* 12 (no. 7) (2022), <https://doi.org/10.3390/app12073491>.
- [67] L.Y. Chung, "The antioxidant properties of garlic compounds: alyl cysteine, alliin, alliin, alliin, and allyl disulfide, *J. Med. Food* 9 (2) (2006) 205–213, <https://doi.org/10.1089/jmf.2006.9.205>.
- [68] Q. Liu, Y.X. Li, J. Qiu, M. Chen, J. Wang, J. Hu, "Antibacterial property and bioadaptability of Ti6Al4V alloy with a silvered gradient nanostructured surface layer, *Rare Met.* 41 (2) (2022) 621–629, <https://doi.org/10.1007/s12598-021-01818-w>.
- [69] Y. Li, et al., "Enhanced antibacterial properties of orthopedic implants by titanium nanotube surface modification: a review of current techniques," *International Journal of Nanomedicine*, Dove Medical Press Ltd 14 (2019) 7217–7236, <https://doi.org/10.2147/IJN.S216175>.
- [70] W.T. Lin, et al., "Inhibited bacterial biofilm formation and improved osteogenic activity on gentamicin-loaded titania nanotubes with various diameters, *Int J Nanomedicine* 9 (1) (2014) 1215–1230, <https://doi.org/10.2147/IJN.S57875>.
- [71] E. Abiy, A. Berhe, "Anti-Bacterial effect of garlic (*Allium sativum*) against clinical isolates of *Staphylococcus aureus* and *Escherichia coli* from patients attending hawassa referral hospital, *Ethiopia, Journal of Infectious Diseases and Treatment* 2 (no. 02) (2016), <https://doi.org/10.21767/2472-1093.100023>.
- [72] A.J. Sales, A. Shadi-Dizaji, Evaluation of inhibitory effect of methanol extract of *Allium sativum* in vitro on *Staphylococcus aureus* and *Escherichia coli* [Online]. Available: <http://sjnmp.muk.ac.ir/article>, 2019.
- [73] M. Kshirsagar, et al., Antibacterial activity of garlic extract on cariogenic bacteria: an in vitro study, *AYU (An international quarterly journal of research in Ayurveda)* 39 (3) (2018) 165, <https://doi.org/10.4103/ayu.ayu.193.16>.
- [74] A. Magryś, A. Olender, D. Tchorzewska, Antibacterial properties of *Allium sativum* L. against the most emerging multidrug-resistant bacteria and its synergy with antibiotics, *Arch. Microbiol.* 203 (5) (2021) 2257–2268, <https://doi.org/10.1007/s00203-021-02248-z>.
- [75] M. Mohammed, M. A. Alhoot, M. F. Mohammed, N. Raman, M. A. Alhoot, and R. Alwan, "Antibacterial Activities of *Allium Sativum* (Garlic) Extracts Against *Staphylococcus Aureus* and *Escherichia Coli*." [Online]. Available: <https://www.researchgate.net/publication/347966738>.
- [76] O.M. Oyawoye, et al., "Antioxidant potential and antibacterial activities of *Allium cepa* (onion) and *Allium sativum* (garlic) against the multidrug resistance bacteria, *Bull. Natl. Res. Cent.* 46 (no. 1) (2022), <https://doi.org/10.1186/s42269-022-00908-8>.
- [77] C. Shuai, C. Shuai, P. Feng, C. Gao, S. Peng, Y. Yang, "Antibacterial capability, physicochemical properties, and biocompatibility of nTiO₂ incorporated polymeric scaffolds, *Polymers* 10 (no. 3) (2018), <https://doi.org/10.3390/polym10030328>. Basel.
- [78] R. Aguirre Ocampo, M. Echeverry-Rendón, S. Robledo, F. Echeverría Echeverría, "Effect of TiO₂ nanotubes size, heat treatment, and UV irradiation on osteoblast behavior, *Mater. Chem. Phys.* 275 (2022), <https://doi.org/10.1016/j.matchemphys.2021.125137>.
- [79] J.S. Khaw, C.R. Bowen, S.H. Cartmell, "Effect of tio₂ nanotube pore diameter on human mesenchymal stem cells and human osteoblasts, *Nanomaterials* 10 (11) (2020) 1–17, <https://doi.org/10.3390/nano10112117>.
- [80] V. Vanitha, S. Vijayakumar, M. Nilavukkarasi, V.N. Punitha, E. Vidhya, P.K. Praseetha, "Heneicosane—a novel microbicidal bioactive alkane identified from *Plumbago zeylanica* L., *Ind. Crops Prod.* 154 (2020), <https://doi.org/10.1016/j.indcrop.2020.112748>.
- [81] Y. Wang, H. Qian, "Phthalates and their impacts on human health, *Healthcare (Switzerland)* 9 (no. 5) (2021), <https://doi.org/10.3390/healthcare9050603>. MDPI AG.
- [82] L. Huang, et al., "Phthalic acid esters: natural sources and biological activities, *Toxins* 13 (no. 7) (2021), <https://doi.org/10.3390/toxins13070495>. MDPI AG.